# Dosimetry of interstitial brachytherapy sources: Recommendations of the AAPM Radiation Therapy Committee Task Group No. 43

Ravinder Nath
*Department of Therapeutic Radiology, Yale University School of Medicine, New Haven, Connecticut 06510*

Lowell L. Anderson
*Department of Medical Physics, Memorial Sloan-Kettering Cancer Center, New York 10021*

Gary Luxton
*Department of Radiation Oncology, University of Southern California, Los Angeles, California 90033*

Keith A. Weaver
*Department of Radiation Oncology, University of California, San Francisco, California 94143*

Jeffrey F. Williamson
*Division of Radiation Oncology, Washington University School of Medicine, St. Louis, Missouri 63110*

Ali S. Meigooni
*Department of Radiation Medicine, University of Kentucky, A. B. Chandler Medical Center, Lexington, Kentucky 40536*

## TABLE OF CONTENTS

## I. INTRODUCTION

The dosimetry of sources used in interstitial brachytherapy has been the subject of considerable research in recent years. A number of articles have appeared (Appendix C) introducing revised calibration standards, source strength specification quantities, and dose calculation formalisms. Some of

these articles advocate revision of basic dosimetry data, including dose rate constants, radial dose functions, and anisotropy functions for $^{192}$Ir, $^{125}$I, and $^{103}$Pd sources. In particular, the Interstitial Collaborative Working Group (ICWG), which was sponsored by the National Cancer Institute, has completed its final report.[1] With all these reports appearing in the literature, the medical physics community is faced with a confusing situation regarding the selection of dosimetry data. Therefore, the Radiation Therapy Committee of the American Association of Physicists in Medicine (AAPM) in 1988 formed Task Group No. 43 to review the recent publications on the dosimetry of interstitial brachytherapy sources and recommend a dosimetry protocol which would include a formalism for dose calculations and a data set for the values of dosimetry parameters. In this final report of the task group, which has been approved by the AAPM Radiation Therapy Committee and the AAPM Science Council, we present a formalism that clearly defines the necessary physical quantities, some of which have been introduced recently, for example, air kerma strength, radial dose function, anisotropy function, dose rate constant, etc. All the equations required for the calculation of dose from a single source using these quantities are also presented. A detailed review of previous studies on the dosimetry of $^{125}$I, $^{192}$Ir, and $^{103}$Pd is presented as an appendix to this report (Appendix C). Relationship of the recommended dose calculation formalism to source strength quantities other than air kerma strength is explained in Appendix A. Also, the relationships between the recommended formalism and other formalisms are briefly described in Appendix B. A glossary of definitions and units is presented in Appendix D. Many readers who may not be experts in brachytherapy physics would find that reading the appendices first makes it easier to follow the recommendations presented in the main body of the text.

Because dose estimates are often made on the basis of exposure calculated from activity, the exposure rate constant has continued to be a matter of interest, although it will be of much less interest when source strengths are routinely specified as air kerma strength. Prior to 1978, exposure rate constants reported for $^{192}$Ir ranged from 3.9 to 5.0 R cm$^2$ mCi$^{-1}$ h$^{-1}$, providing a good example of why it is poor practice to specify source strength as activity, since the activity might be inferred by the manufacturer using one value of the constant and the dose might be calculated by the user from a different value. In part, because of these reasons, the recommendations in this report include a new dose calculation formalism for the dosimetry of interstitial brachytherapy sources. Several new quantities have been introduced, which differ conceptually from the quantities currently in use. For example, gamma ray constant, exposure rate constant, tissue attenuation factors, apparent activity, and exposure-to-dose conversion factors are not needed in the new formalism. Instead, only quantities directly derived from dose rates in water medium near the actual source are used. Some of these quantities are dose rate constant, radial dose function, anisotropy function, anisotropy factor, and geometry factor. Recommended values of dosimetry constants would result in changes of up to 17% in the dosimetry of interstitial brachytherapy sources. A qualified brachytherapy

TABLE I. Physical characteristics of $^{192}$Ir radionuclide.

Decay modes (Ref. 1):
$\beta$   decay to excited states of $^{192}$Pt (95.6%)
Electron capture to excited states of $^{192}$Os (4.4%)

Energy of major gamma rays—MeV (number of photons per decay) (Ref. 1):
0.29 (.291), 0.308 (.298), 0.317 (.831), 0.468 (.476), 0.608 (.133)

Average number of gamma rays per decay (Ref. 1): 2.2

Half life of ground state (Ref. 2):
73.83 days

Exposure rate and air kerma rate constants for ideal point source (Ref. 3):
$(\Gamma_\delta)_x = 4.69$ R cm$^2$ mCi$^{-1}$ h$^{-1}$
$(\Gamma_\delta)_k = 0.111$ $\mu$Gy m$^2$ MBq$^{-1}$ h$^{-1}$
$= 4.11$ cGy cm$^2$ mCi$^{-1}$ h$^{-1}$
$= 1.00$ cGy cm$^2$ U$^{-1}$ h$^{-1}$

physicist should carefully assess the implications of this report for clinical dose prescription, and review these findings with the responsible radiation oncologist before implementing this protocol. The recommended formalism can be applied to both high and low dose rate remotely afterloaded brachytherapy as well as the manually afterloading sources covered by this report. However, no data is included in the text because consensus data on the dosimetry of remotely afterloadable brachytherapy sources are not available yet.

## II. DESCRIPTION OF SOURCES

Traditionally, interstitial implants were performed with $^{226}$Ra needles. Due to radiation safety considerations, however, $^{226}$Ra has largely been replaced with other radionuclides and will not be discussed further. Today the vast majority of interstitial brachytherapy treatments in North America are done using either $^{192}$Ir or $^{125}$I sources. Recently $^{103}$Pd sources have also become available for permanent implants. A description of $^{192}$Ir, $^{125}$I, and $^{103}$Pd interstitial sources is given in the following sections. Source strengths are stated in units of air kerma strength, which is defined in Sec. III A, and is denoted in this report by the symbol U.

### A. Iridium-192 sources

$^{192}$Ir is produced when stable $^{191}$Ir (37% abundance) absorbs a neutron. It decays with a 73.83 day half life to several excited states of $^{192}$Pt and $^{192}$Os, which emit gamma rays with a range of energies (see Table I). The average energy of the emitted photons from an unencapsulated source is about 370 keV (Attix and Goetch argue that the appropriate mean energy for ion chamber calibration factor interpolation and other dosimetric purposes is the energy-fluence weighted average with suppression of the very low energy components that are absorbed by the source and its encapsulation; for $^{192}$Ir, they recommend a value of 400 keV).

In the United States $^{192}$Ir used for interstitial radiotherapy is usually in the form of small cylindrical sources or "seeds." These are 3 mm long and 0.5 mm in diameter. Two seed styles are commercially available: one (manufactured by Best Industries, Springfield, VA) has a 0.1 mm diameter core of 30% Ir–70% Pt surrounded by a 0.2 mm thick clad-

TABLE II. Physical characteristics of $^{125}I$ radionuclide.

Decay modes (Ref. 1):
    Electron capture to first excited state of $^{125}Te$
    De-excitation via gamma emission (7%) and internal conversion (93%)
    Fluorescent x rays following electron capture and internal conversion

Energy of emitted photons—keV (number of photons per decay) (Ref. 1):
    27.4 (1.15), 31.4 (0.25), 35.5 (0.067)

Average number of photons per decay (Ref. 1): 1.4

Half life (Ref. 4): 59.4 days

Exposure rate and air kerma rate constants for ideal point source:[a]
    $(\Gamma_\delta)_x = 1.51$ R cm$^2$ mCi$^{-1}$ h$^{-1}$
    $(\Gamma_\delta)_k = 0.0358$ $\mu$Gy m$^2$ MBq$^{-1}$ h$^{-1}$
    $= 1.32$ cGy cm$^2$ mCi$^{-1}$ h$^{-1}$
    $= 1.00$ cGy cm$^2$ U$^{-1}$ h$^{-1}$

[a]Derived from Ref. 5 using an updated value of $(W/e) = 0.876$ cGy R$^{-1}$. In interpreting vendor calibration certificates, the $(\Gamma_\delta)_x$ value of 1.45 R cm$^2$ mCi$^{-1}$ h$^{-1}$ is used by convention.

ding of stainless steel. The other (manufactured by Alpha-Omega, Bellflower, CA) has a 0.3 mm diameter core of 10% Ir–90% Pt surrounded by a 0.1 mm thick cladding of Pt. The seeds are supplied inside strands of nylon of 0.8 mm outside diameter. While the normal center-to-center source spacing is 1 cm, custom spacings are also available. The maximum active strand length is about 18 cm. Air kerma strengths ranging from 1.4–7.2 U (equivalent to an $M_{eq}$ value of 0.2–1.0 mgRaEq; units of U are defined in Sec. III A 2) are commonly available, and some suppliers can provide strengths up to 72 U (equivalent to an $M_{eq}$ value of 10 mgRaEq). Dosimetry data presented in this report applies to the stainless-steel-clad $^{192}Ir$ sources only, because similar quality data are not currently available for the platinum-encapsulated $^{192}Ir$ seeds.

In Europe $^{192}Ir$ is most commonly used in the form of wire. Typically the wires are made from a 25% Ir–75% Pt core surrounded by a 0.1 mm thick Pt cladding. Outside diameters of 0.3 mm and about 0.55 mm are available. The thicker wire can be inserted directly into tissue, while the thinner wire, encased in a plastic covering, is afterloaded in implanted catheters. Also, several manufacturers market high dose rate interstitial afterloaders that employ a single $^{192}Ir$ source of air kerma strength 29 000–41 000 U (7–10 Ci). Dosimetry of $^{192}Ir$ wire and high activity sources for remote afterloaders is beyond the scope of this report and recommendations about this modality are not presented here.

## B. Iodine-125 sources

$^{125}I$ is produced when $^{124}Xe$ absorbs a neutron, and then decays via electron capture. $^{125}I$ itself decays with a half life of 59.4 days, by electron capture to the first excited state of $^{125}Te$, which undergoes internal conversion 93% of the time and otherwise emits a 35.5 keV gamma ray. The electron capture and internal conversion processes give rise to characteristic x rays, listed in Table II.

$^{125}I$ for interstitial implants is available commercially in the form of small "seed" sources. Three models are available. Two of these seed types, manufactured by 3M until

recently, are now marketed by the Medi-Physics Division (Arlington Heights, IL) of Amersham. Both of these seeds are 4.5 mm long, 0.8 mm in diameter, and have a 0.05 mm thick titanium wall, sealed by end welds. Internally, one model (6711) contains a silver wire of about 3 mm length with the active material as silver iodide on the surface. This model is available in air kerma strengths up to 6.3 U (equivalent to an apparent activity of 5 mCi). The other model (6702) contains the radioisotope absorbed in 3–5 tiny resin spheres, and is available with strengths up to 51 U (equivalent to an apparent activity of 40 mCi). Model 6711 seed also emits silver characteristic x rays with energies of 22.1 and 25.5 keV. For this seed the average photon energy is about 27.4 keV, whereas model 6702 emits photons with an average energy of 28.5 keV. Both seed models are available as loose seeds; additionally the low activity model is also available as strands of 10 seeds spaced 1 cm apart in absorbable suture.

In this report, no data are presented on the newly introduced double-walled $^{125}I$ model 2300 source now marketed by Best Industries.

## C. Palladium-103 sources

$^{103}Pd$ is formed when stable $^{102}Pd$ absorbs a neutron. It decays via electron capture, mostly to the first and second excited states of $^{103}Rh$, with a 17.0 day half life. De-excitation is almost totally via internal conversion, leading to the production of characteristic x rays. Average photon energy is about 21 keV. Table III summarizes the decay properties.

$^{103}Pd$ sources are similar in size and encapsulation to $^{125}I$ sources, being 4.5 mm long and 0.8 mm in diameter. The $^{103}Pd$ is encapsulated in a 0.05 mm thick titanium tube that is laser welded on the ends. The active material is coated onto two graphite pellets 0.9 mm long and 0.6 mm in diameter. Between the active pellets is a 1 mm long lead marker that provides good source visibility on radiographs. Air kerma strengths up to 2.6 U (equivalent to an apparent activity of 2 mCi) are normally available.

## III. RECOMMENDED DOSE CALCULATION FORMALISM

The recommended protocol is based on measured (or measurable) quantities and decouples a number of interrelated quantities. It also allows calculations of two-dimensional dose distributions around interstitial sources. The dosimetry data endorsed by this report results in absolute dose rate changes as large as 17% relative to conventionally used treatment planning data.[1,6–10] Therefore, careful attention should be paid to the clinical impact of these recommendations.

The dose calculation formalism proposed here, in contrast to traditional methods using exposure rate constants and tissue attenuation factors, requires input data consisting of dose rates from an actual source in a tissue equivalent phantom. Traditionally, dose rate $\dot{D}(r)$ at a distance $r$ from an interstitial brachytherapy source is calculated using the point-source approximation

$$\dot{D}(r) = A_{app} f_{med} (\Gamma_\delta)_x (1/r^2) T(r) \bar{\phi}_{an}, \tag{1}$$

TABLE III. Physical characteristics of $^{103}$Pd radionuclide.

Decay modes (Ref. 1):
  Electron capture to excited states of $^{103}$Rh
  De-excitation via gamma emission and internal conversion
  Fluorescent x rays following electron capture and internal conversion

Energy of principal emitted photons—keV (number of photons per decay) (Ref. 1):
  20.1 (.656), 23.0 (.125)

Average number of photons per decay (Ref. 1): 0.8

Half life (Ref. 11): 16.97 days

Exposure rate and air kerma rate constants for ideal point source (Ref. 12): $1.14 \ \mathrm{R \ cm^2 \ h^{-1} \ U^{-1}}$
  $(\Gamma_\delta)_x = 1.48 \ \mathrm{R \ cm^2 \ mCi^{-1} \ h^{-1}}$
  $(\Gamma_\delta)_k = 0.0350 \ \mathrm{\mu Gy \ m^2 \ MBq^{-1} \ h^{-1}}$
    $= 1.296 \ \mathrm{cGy \ cm^2 \ mCi^{-1} \ h^{-1}}$
    $= 1.00 \ \mathrm{cGy \ cm^2 \ U^{-1} \ h^{-1}}$

where $A_{app}$ is the apparent activity of the source;

$f_{med}$ is the exposure-to-dose conversion factor;

$(\Gamma_\delta)_x$ is the exposure rate constant for the radionuclide in the source;

$T(r)$ is the tissue attenuation factor as defined by Eq. (B5) in Appendix B;

$\phi_{an}$ is the anisotropy constant. The new approach follows the recommendation of the ICWG (Chap. 3).[1] In the recommended protocol each of the quantities used to calculate absorbed dose rate is measured or calculated for the specific type of source in question and therefore depends on source construction and geometry in addition to the primary photon spectrum and medium. In contrast, much of the input data to the older semianalytical models, including exposure rate constants and buildup factors, are fundamental properties of the radionuclide.

One of the fundamental problems with the older protocols is that they are based upon photon fluence around the source in free space, whereas clinical applications require dose distributions in a scattering medium such as a patient. Determination of two-dimensional dose distributions in a scattering medium from a knowledge of the two-dimensional distribution of photon fluence in free space is easily accomplished only for a point isotropic source. An actual brachytherapy source exhibits considerable anisotropy and for such sources it is all but impossible to determine accurately dose distributions in a scattering medium from distributions of photon fluence in free space. The recommended formalism solves this fundamental problem by a direct use of measured or measurable dose distributions produced by a source in a water equivalent medium.

The recommended protocol introduces or utilizes a number of new quantities such as the anisotropy function, $F(r, \theta)$; dose rate constant, $\wedge$; geometry factor, $G(r, \theta)$; radial dose function, $g(r)$; and air kerma strength, $S_k$. All of these quantities are properly defined in Section III A. These quantities replace the following familiar quantities:

  apparent activity, $A_{app} \rightarrow$ air kerma strength, $S_k$,
  exposure rate constant, $(\Gamma_\delta)_x \rightarrow$ dose rate constant, $\wedge$,
  inverse square distance, $(1/r^2) \rightarrow$ geometry factor, $G(r, \theta)$ [for 2-D calculations only],
  tissue attenuation factor, $T(r) \rightarrow$ radial dose function, $g(r)$.

anisotropy constant, $\bar{\phi}_{an} \rightarrow$ anisotropy function, $F(r, \theta)$ [for 2-D calculations only].

The recommended protocol allows for two-dimensional dose calculations around cylindrically symmetric sources whereas the old protocol could handle one-dimensional, point isotropic sources only. In order to address full 2-D calculations, two new functions of $r$ and $\theta$ are introduced: the geometry factor, $G(r, \theta)$, accounts for the dependence of photon fluence around a source in free space; and the anisotropy function, $F(r, \theta)$, accounts for anisotropy of dose distribution produced by a source in a scattering medium. Whereas the radial dose function, $g(r)$, accounts for the depth dependence of dose in a scattering medium along the transverse axis of the source, the anisotropy function, $F(r, \theta)$, accounts for anisotropy of dose relative to dose on the transverse axis. We chose to decouple various physical factors by introducing radial dose function $g(r)$ and anisotropy function $F(r, \theta)$; both of which are relative quantities. Because of their relative nature, the uncertainties in their determinations are reduced. The only quantity in the new formalism retaining units of absolute dose rate is the dose rate constant $\wedge$. Another advantage of this decoupling is that when more accurate values for anisotropy function $F(r, \theta)$ or radial dose function $g(r)$ become available from better measurements or future calculations, they can be easily accommodated in a revision of the protocol.

## A. General formalism for two-dimensional case

We restrict consideration to cylindrically symmetric sources, such as that illustrated in Fig. 1. For such sources, the dose distribution is two-dimensional and can be described in terms of a polar coordinate system with its origin at the source center where $r$ is the distance to the point of interest and $\theta$ is the angle with respect to the long axis of the source (Fig. 1). The dose rate, $\dot{D}(r, \theta)$, at point $(r, \theta)$ can be written as

$$\dot{D}(r, \theta) = S_k \wedge [G(r, \theta)/G(r_0, \theta_0)]g(r)F(r, \theta), \qquad (2)$$

where $S_k = $ air kerma strength of the source (defined in Sec. III A 2);

$\wedge = $ dose rate constant (defined in Sec. III A 3 in units of $\mathrm{cGy \ h^{-1} \ U^{-1}}$);
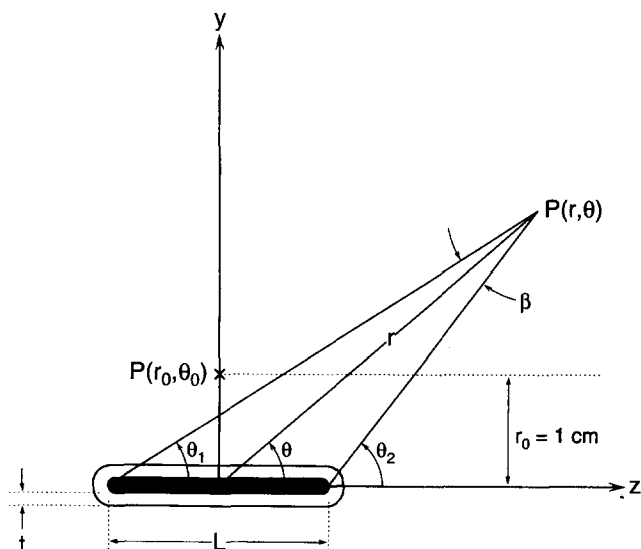
FIG. 1. Illustration of geometry assumed in the dose calculation formalism. Angle $\beta$ is that subtended by the active length at point $P$. The reference point is represented by $P(r_0, \theta_0)$.

$G(r, \theta)$ = geometry factor (defined in Sec. III A 4);

$g(r)$ = radial dose function (defined in Sec. III A 5);

$F(r, \theta)$ = anisotropy function (defined in Sec. III A 6); and each of these quantities or functions and the reference point $(r_0, \theta_0)$ are described below.

## 1. Reference point for dose calculations

The reference point $(r_0, \theta_0)$ is chosen in this report to lie on the transverse bisector of the source at a distance of 1 cm from its center, i.e., $r_0 = 1$ cm and $\theta_0 = \pi/2$. This choice of reference point for dose calculation in a medium is consistent with the traditional practice of using a distance of 1 cm from the source as a reference point.

## 2. Air kerma strength, $S_k$

Air kerma strength is a measure of brachytherapy source strength, which is specified in terms of air kerma rate at the point along the transverse axis of the source in free space. It is defined[13] as the product of air kerma rate at a calibration distance, $d$, in free space, $\dot{K}(d)$, measured along the transverse bisector of the source, and the square of the distance, $d$

$$S_k = \dot{K}(d)d^2. \tag{3}$$

The calibration distance $d$ must be large enough that the source may be treated as a mathematical point. In actual practice, air kerma rate standardization measurements are performed in air and corrections for air attenuation are applied if needed. Whereas the measurements for source strength calibration may be performed at any large distance, $d$, it is customary to specify the air kerma strength in terms of a reference calibration distance, $d_0$, which is usually chosen to be 1 m. It should be noted that the user typically does not perform the in-air calibration, which is primarily performed by the standardization laboratories (National Institute of Standards and Technology, NIST, and accredited dosime-

try calibration laboratories, ADCLs in the USA and the National Research Council of Canada). However, it is the responsibility of the user to verify the accuracy of source strength provided by the vendor. Typically, the user has a well-type ionization chamber that has a calibration traceable to the national standards for each type of brachytherapy source.

If kerma, time, and distance are assigned units of $\mu$Gy, h, and m, respectively, $S_k$ will have units $\mu$Gy m$^2$ h$^{-1}$ as recommended by the TG-32 report.[13] In this report, this unit is denoted by the symbol U, that is,

1  U = 1  unit of air kerma strength

$$= 1 \ \mu Gy \ m^2 \ h^{-1} = 1 \ cGy \ cm^2 \ h^{-1}. \tag{4}$$

The conversion factors needed to renormalize Eq. (1) for alternative source strength specifications are discussed in Appendix A and are summarized in Table IV. The geometric relationship between the point of output determination and an arbitrary filtered source and other details have been described previously by Williamson and Nath.[14]

## 3. Dose rate constant, $\wedge$

The dose rate constant is defined as the dose rate to water at a distance of 1 cm on the tranverse axis of a unit air kerma strength source in a water phantom. It should be noted that $\wedge$ is an absolute quantity, unlike others that follow in this section, which are normalized (relative) quantities. For specification of the dose rate constant as well as relative dose distribution parameters, this report recommends that liquid water be accepted as the reference medium. In determining the value of $\wedge$, the 1 cm distance is specified along the transverse axis of the actual source (rather than an idealized point source) relative to its geometric center. Mathematically, the dose rate constant, $\wedge$, is

$$\wedge = \dot{D}(r_0, \theta_0)/S_K. \tag{5}$$

The constant includes the effects of source geometry, the spatial distribution of radioactivity within the source, encapsulation, and self-filtration within the source and scattering in water surrounding the source. The numerical value of this quantity also depends on the standardization measurements to which the air kerma strength calibration of the source is traceable; in other words, if the air kerma strength standard for a given source provided by NIST is changed in the future, the value of $\wedge$ will also change. The relationship of $\wedge$ to related quantities such as exposure rate constant is discussed in Appendix B.

## 4. Geometry factor, $G(r, \theta)$

The geometry factor accounts for the variation of relative dose due only to the spatial distribution of activity within the source, ignoring photon absorption and scattering in the source structure. It is defined as

$$G(r, \theta) = \frac{\int_V [\rho(r')dV'/|r' - r|^2]}{\int_V \rho(r')dV'}, \tag{6}$$

where $\rho(r')$ represents the density of radioactivity at the point $p(r') = p(x', y', z')$ within the source and $V$ denotes

TABLE IV. Source strength conversion factors for interstitial brachytherapy sources.[a]

| Sources | Source strength quantity | Units | Exposure rate constant $(\Gamma \delta)_x$ or exposure rate constant for filtration $(\Gamma \delta)_{x,f}$ R cm$^2$ mCi$^{-1}$ h$^{-1}$ | Air kerma strength conversion factor $(S_k$/quantity) |
|---|---|---|---|---|
| All | Equivalent mass of Radium | mgRaEq | 8.25 | 7.227 U mgRaEq$^{-1}$ |
| All | Reference exposure rate | mR m$^2$ h$^{-1}$ | $\cdots$ | 8.760 U/mR m$^2$ h$^{-1}$ |
| | | nR m$^2$ s$^{-1}$ | $\cdots$ | 3.154×10$^{-2}$ |
| | | C kg$^{-1}$ m$^2$ s$^{-1}$ | $\cdots$ | U/nR m$^2$ s$^{-1}$ 1.222× 10$^{11}$ U/C kg$^{-1}$ m$^2$ s$^{-1}$ |
| $^{192}$Ir seed $t$=0.2 mm Fe | Apparent activity | mCi | 4.60 | 4.030 U mCi$^{-1}$ |
| $^{192}$Ir seed $t$=0.05 mm Pt–Ir | Apparent activity | mCi | 4.80[b] | 4.205 U mCi$^{-1}$ |
| $^{125}$I seeds | Apparent activity | mCi | 1.45 | 1.270 U mCi$^{-1}$ |
| $^{103}$Pd seeds | Apparent activity | mCi | 1.48 | 1.293 U mCi$^{-1}$ |

[a]Data from Williamson and Nath (Ref. 14).
[b]See the explanation for using 4.80 vs 4.60 in Ref. 14. Briefly, the manufacturer uses 4.80 in calibrating their sources, therefore the user must also use the same number.

integration over the source core. $dV'$ is a volume element located at $r'$ in the source. Because the three-dimensional distribution of $\rho(\mathbf{r})$ is uncertain for many sources such as $^{125}$I and because the choice of $G(r,\theta)$ influences only the accuracy of interpolation (as explained further in Sec. III A 6), the line source approximation to $G(r,\theta)$ has been selected for use in this report. When the distribution of radioactivity can be approximated by a point source or by a line source of length, $L$, then $G(r,\theta)$ reduces to

$$G(r,\theta)=\begin{cases} r^{-2}, & \text{for point source approximation} \\ \dfrac{\beta}{Lr\sin\theta}, & \text{for line source approximation} \end{cases}$$

(7)

where $L$ is the active length of the source, and $\beta$ is the angle subtended by the active source with respect to the point $(r,\theta)$ (see Fig. 1); i.e., $\beta=\theta_2-\theta_1$. $G(r,\theta)$ represents the hypothetical relative dose distribution due only to the spatial distribution of radioactivity and ignores the effects of absorption and scattering in the source or the surrounding medium. Values of $G(r,\theta)$ for a 3 mm line source are given in Table V.

## 5. Radial dose function, g(r)

The radial dose function, $g(r)$, accounts for the effects of absorption and scatter in the medium along the transverse axis of the source. It is defined as

$$g(r)=\dot{D}(r,\theta_0)G(r_0,\theta_0)/\dot{D}(r_0,\theta_0)G(r,\theta_0).$$

(8)

The radial dose function applies only to transverse axis, i.e., only for points with an angle of $\theta_0$, which is equal to $\pi/2$. This function defines the falloff of dose rate along the trans-

verse axis due to absorption and scattering in the medium. It can also be influenced by filtration of photons by the encapsulation and source materials.

The function $g(r)$ is similar to a normalized transverse-axis tissue-attenuation factor or absorbed dose to kerma in free space ratio, as explained in Appendix B. It should be noted that the above definition of radial dose function is different from the older (Dale's)[15–17] definition, as explained in Appendix B 3.

## 6. Anisotropy function, F(r,θ)

The anisotropy function accounts for the anisotropy of dose distribution around the source, including the effects of absorption and scatter in the medium. It is defined as

$$F(r,\theta)=\dot{D}(r,\theta)G(r,\theta_0)/\dot{D}(r,\theta_0)G(r,\theta).$$

(9)

This two-dimensional function gives the angular variation of dose rate about the source at each distance due to self-filtration, oblique filtration of primary photons through the

TABLE V. Example of the geometry factor, $G(r,\theta)$ times $r^2$, for a seed approximated by 3.0 mm line source as calculated with Eq. (7).

| $\theta$(deg) | $r$=0.5 cm | $r$=1.0 cm | $r$=2.0 cm | $r$=5.0 cm |
|---|---|---|---|---|
| 0 | 1.099 | 1.023 | 1.006 | 1.001 |
| 10 | 1.094 | 1.022 | 1.006 | 1.001 |
| 20 | 1.081 | 1.019 | 1.005 | 1.001 |
| 30 | 1.062 | 1.015 | 1.004 | 1.001 |
| 40 | 1.039 | 1.010 | 1.002 | 1.001 |
| 50 | 1.018 | 1.005 | 1.001 | 1.000 |
| 60 | 0.9160 | 0.9999 | 1.000 | 1.000 |
| 90 | 0.9715 | 0.9926 | 0.9980 | 1.000 |

encapsulating material, and scattering of photons in the medium. The role of the geometry factor in Eq. (8) is to suppress the influence of inverse square law on the dose distribution around the source.

Due to the large dose rate gradients encountered near interstitial sources, it is difficult to measure dose rates accurately at distances less than 5 mm from the source. In addition, the large dose rate variation arising from inverse square law makes accurate interpolation of intermediate dose rate values difficult without an excessively large table of measured data. By suppressing inverse square law effects, extrapolation to small distances from dose rate profiles measured at distances of 5 and 10 mm as well as interpolation between sparsely distributed measured values is usually more accurate.

## B. Point isotropic source approximation

Some clinical treatment planning systems for interstitial brachytherapy utilize the one-dimensional isotropic point-source model to compute interstitial source dose distributions. In this approximation, dose depends only on the radial distance from the source. If a large number of seeds are randomly oriented, or the degree of dose anisotropy around single sources is limited, the dose rate contribution to tissue from each seed can be well approximated by the average radial dose rate as estimated by integrating the single anisotropic seed source with respect to solid angle.

$$\dot{D}(r) = \frac{1}{4\pi} \int_0^{4\pi} \dot{D}(r,\theta)d\Omega, \tag{10}$$

where $d\Omega = 2\pi \sin\theta d\theta$ for a cylindrically symmetric dose distribution.

### 1. Anisotropy factor, $\phi_{an}(r)$

Substituting Eq. (2) into Eq. (10) and rearranging, leads to

$$\dot{D}(r) = S_k \Lambda \frac{G(r,\theta_0)}{G(r_0,\theta_0)} g(r)\phi_{an}(r), \tag{11}$$

where $\phi_{an}(r)$ is the anisotropy factor

$$\phi_{an}(r) = \frac{\int_0^\pi \dot{D}(r,\theta)\sin\theta d\theta}{2\dot{D}(r,\theta_0)}. \tag{12}$$

The factor $\phi_{an}(r)$ is the ratio of the dose rate at distance $r$, averaged with respect to solid angle, to dose rate on the transverse axis at the same distance. For the sources considered in this report, $\phi(r)$ is less than 1, having values ranging from 0.91 to 0.97 depending upon the source (for detailed data, see the next section). For distances greater than the source active length, the equation for dose around a source using point-source approximation can be simplified to

$$\dot{D}(r) = (S_k \Lambda/r^2)g(r)\phi_{an}(r). \tag{13}$$

### 2. Anisotropy constant, $\bar{\phi}_{an}$

For the sources considered in this report, the anisotropy factor, $\phi(r)$, may be approximated by a distance-independent constant, $\bar{\phi}_{an}$, which we call the anisotropy constant, which usually takes a value less than 1.00. Thus, the anisotropy factor, $\phi_{an}(r)$, in Eq. (13) can be replaced by a

constant $\bar{\phi}_{an}$ without a significant loss in accuracy. It should be noted that point source approximation [i.e., Eq. (12) or (13)] gives a dose rate at the reference point in the medium on the transverse bisector at a distance of 1 cm from the source, equal to $\Lambda \phi_{an}(r)$ for a unit air kerma strength source. Thus, dose rate on the transverse axis in the medium is somewhat lower using the point-source approximation than the actual dose rate by 3% to 9% for the sources considered in this report.

Table VI. Recommended dose rate constants in a water medium.

| Seed | cGy hr$^{-1}$ U$^{-1}$ |
|---|---|
| $^{192}$Ir[a] | 1.12 |
| Fe Clad | |
| $^{125}$I Model 6702[a] | 0.93 |
| $^{125}$I Model 6711[a] | 0.88 |
| $^{103}$Pd[b] | 0.74 |
| Model 200 | |

[a]Data from Williamson (Ref. 18).
[b]Data from Meigooni, Sabnis, and Nath (Ref. 12) and Chiu-Tsao and Anderson (Ref. 19) were averaged and then multiplied by 1.048 (Ref. 18), a correction factor for converting Solid Water data to water, as calculated by Williamson using Monte Carlo simulation (Ref. 18).

Table VII. Radial dose functions, $g(r)$.

| Distance along transverse axis (cm) | Radial dose function, $g(r)$ | | | |
|---|---|---|---|---|
| | $^{103}$Pd[b] | $^{126}$I Model 6711[a] | $^{125}$I Model 6702[a] | $^{192}$Ir[a] |
| 0.5 | 1.29 | 1.04 | 1.04 | 0.994 |
| 1.0 | 1.00 | 1.00 | 1.00 | 1.00 |
| 1.5 | 0.765 | 0.926 | 0.934 | 1.01 |
| 2.0 | 0.576 | 0.832 | 0.851 | 1.01 |
| 2.5 | 0.425 | 0.731 | 0.760 | 1.01 |
| 3.0 | 0.310 | 0.632 | 0.670 | 1.02 |
| 3.5 | 0.224 | 0.541 | 0.586 | 1.01 |
| 4.0 | 0.165 | 0.463 | 0.511 | 1.01 |
| 4.5 | 0.123 | 0.397 | 0.445 | 1.00 |
| 5.0 | 0.0893 | 0.344 | 0.389 | 0.996 |
| 5.5 | | 0.300 | 0.341 | 0.985 |
| 6.0 | | 0.264 | 0.301 | 0.972 |
| 6.5 | | 0.233 | 0.266 | 0.957 |
| 7.0 | | 0.204 | 0.235 | 0.942 |
| 7.5 | | | | 0.927 |
| 8.0 | | | | 0.913 |
| 8.5 | | | | 0.900 |
| 9.0 | | | | 0.891 |

[a]Radial dose functions of $^{125}$I sources were fit to a 5th order polynomial, $g(r)=a_0+a_1r+a_2r^2+a_3r^3+a_4r^4+a_5r^5$. Coefficients of the fit for $^{125}$I Model 6711 were $a_0=1.013\,76$, $a_1=1.227\,47\times10^{-1}$, $a_2=-1.730\,25\times10^{-1}$, $a_3=4.023\,78\times10^{-2}$, $a_4=-3.852\,27\times10^{-3}$, $a_5=1.342\,83\times10^{-4}$. For $^{125}$I Model 6702, coefficients were $a_0=1.023\,07$, $a_1=8.637\,51\times10^{-2}$, $a_2=-1.371\,55\times10^{-1}$, $a_3=3.077\,95\times10^{-2}$, $a_4=-2.869\,46\times10^{-3}$, $a_5=9.875\,58\times10^{-5}$. Radial dose function of $^{192}$Ir was fit to a 4th order polynomial, $g(r)=a_0+a_1r+a_2r^2+a_3r^3+a_4r^4$. Coefficients were $a_0=9.890\,54\times10^{-1}$, $a_1=8.813\,19\times10^{-3}$, $a_2=3.517\,78\times10^{-3}$, $a_3=-1.466\,37\times10^{-3}$, $a_4=9.243\,70\times10^{-5}$.
[b]Data averaged from Meigooni, Sabnis, and Nath (Ref. 12) and Chiu-Tsao and Anderson (Ref. 19). Radial dose function was fit to a 5th order polynomial, $g(r)=a_0+a_1r+a_2r^2+a_3r^3+a_4r^4+a_5r^5$. Coefficients are (for $^{103}$Pd) $a_0=1.628\,91$, $a_1=-7.685\,59\times10^{-1}$, $a_2=1.542\,72\times10^{-1}$, $a_3=-2.271\,85\times10^{-2}$, $a_4=3.393\,30\times10^{-3}$, $a_5=-2.672\,15\times10^{-4}$.
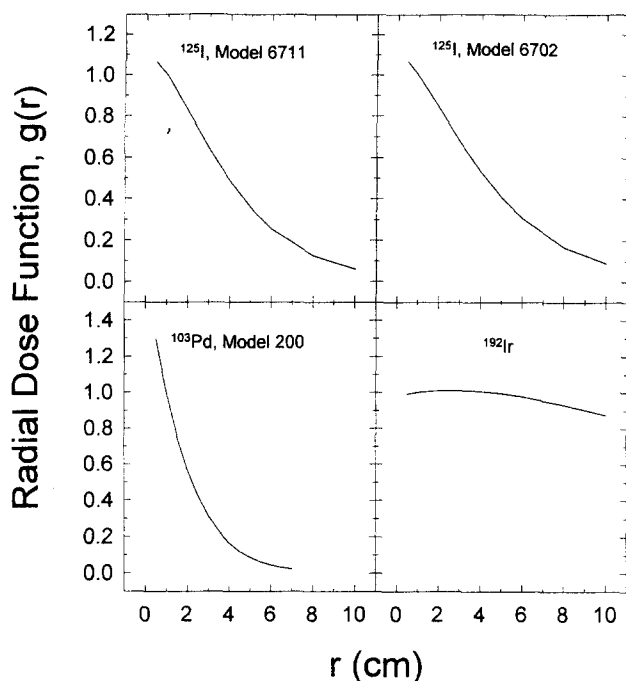
FIG. 2. Radial dose functions in a Solid Water medium for [103]Pd, ^{125}I, and ^{192}Ir sources.



FIG. 4. Anisotropy function, $F(r,\theta)$, in a Solid Water medium for [103]Pd, ^{125}I, and ^{192}Ir sources [reprinted with permission (Ref. 20)].

## IV. RECOMMENDED DOSIMETRY PARAMETERS

### A. Dose rate constant, $\Lambda$

Recommended values of dose rate constants in the water medium are given in Table VI. Dose rate constants for ^{125}I and ^{192}Ir were taken from a recent study by Williamson,[18]
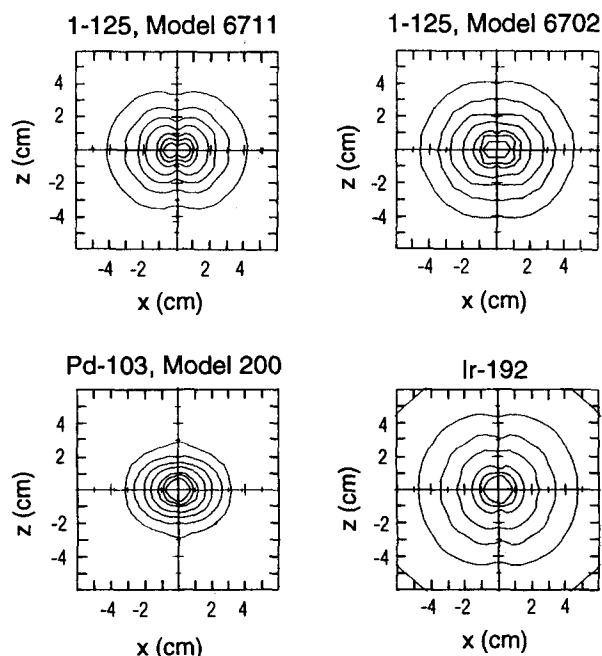


FIG. 3. The isodose curves produced by ^{125}I models 6711 and 6702, [103]Pd and ^{192}Ir sources with air kerma strength of 100 U. The dose rates for the isodose curves starting from the outside were 2, 5, 10, 20, 50, 100, and 200 cGy/h.
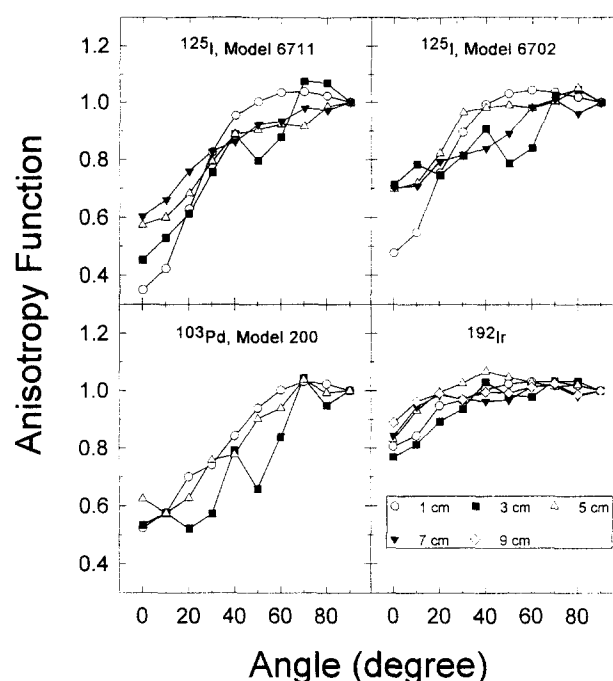
which compares the ICWG (Chap. 3)[1] measured data to Monte Carlo photon transport calculations. For [103]Pd, a similar Monte Carlo study has not yet been satisfactorily completed; the simulations have not been able to reproduce the measured Solid Water™ dose rate constant. However, a relative correction factor for conversion from Solid Water to liquid water has been calculated with good accuracy. Therefore, the dose rate constants measured in Solid Water by Meigooni *et al.*[12] and Chiu-Tsao *et al.*[19] were averaged, and this average value was then multiplied by 1.048, a correction factor obtained from Williamson[18] for converting data in Solid Water to data in water.

### B. Radial dose function, $g(r)$

For ^{125}I and ^{192}Ir, the radial dose functions in a Solid Water medium were taken from the ICWG (Chap. 3).[1] For [103]Pd, the radial dose function in a Solid Water medium from Meigooni *et al.*[12] and Chiu-Tsao *et al.*[19] were averaged. The radial dose functions in a Solid Water medium were fitted to a polynomial series expansion

$$g(r) = a_0 + a_1 r^2 + a_2 r^2 + a_3 r^3 + \cdots . \tag{14}$$

TABLE VIII. Calculated anisotropy function, $F(r,\theta)$, for a [103]Pd Model 200 source.

| $\theta$(deg) $r$(cm) | 0.0 | 10.0 | 20.0 | 30.0 | 40.0 | 50.0 | 60.0 | 70.0 | 80.0 | 90.0 |
|---|---|---|---|---|---|---|---|---|---|---|
| 1.0 | 0.523 | 0.575 | 0.700 | 0.741 | 0.843 | 0.939 | 1.00 | 1.03 | 1.02 | 1.00 |
| 2.0 | 0.526 | 0.544 | 0.590 | 0.615 | 0.748 | 0.876 | 0.962 | 1.08 | 1.06 | 1.00 |
| 3.0 | 0.533 | 0.575 | 0.520 | 0.572 | 0.791 | 0.658 | 0.838 | 1.04 | 0.948 | 1.00 |
| 4.0 | 0.544 | 0.442 | 0.463 | 0.646 | 0.773 | 0.848 | 0.887 | 0.94 | 0.963 | 1.00 |
| 5.0 | 0.624 | 0.574 | 0.627 | 0.758 | 0.777 | 0.901 | 0.939 | 1.04 | 0.992 | 1.00 |

TABLE IX. Calculated anisotropy function, $F(r,\theta)$, for a [125]I Model 6711 source.

| θ(deg) r(cm) | 0.0 | 10.0 | 20.0 | 30.0 | 40.0 | 50.0 | 60.0 | 70.0 | 80.0 | 90.0 |
|---|---|---|---|---|---|---|---|---|---|---|
| 1.0 | 0.350 | 0.423 | 0.628 | 0.826 | 0.953 | 1.00 | 1.03 | 1.04 | 1.02 | 1.00 |
| 2.0 | 0.439 | 0.549 | 0.690 | 0.816 | 0.903 | 0.954 | 1.00 | 1.06 | 1.04 | 1.00 |
| 3.0 | 0.452 | 0.529 | 0.612 | 0.754 | 0.888 | 0.795 | 0.877 | 1.07 | 1.07 | 1.00 |
| 4.0 | 0.521 | 0.582 | 0.688 | 0.798 | 0.842 | 0.866 | 0.935 | 0.969 | 0.998 | 1.00 |
| 5.0 | 0.573 | 0.600 | 0.681 | 0.793 | 0.888 | 0.903 | 0.922 | 0.915 | 0.985 | 1.00 |
| 6.0 | 0.581 | 0.621 | 0.718 | 0.803 | 0.826 | 0.891 | 0.912 | 0.953 | 0.962 | 1.00 |
| 7.0 | 0.603 | 0.660 | 0.758 | 0.829 | 0.861 | 0.922 | 0.932 | 0.978 | 0.972 | 1.00 |

TABLE XI. Calculated anisotropy function, $F(r,\theta)$, for an ^{192}Ir source.

| θ(deg) r(cm) | 0.0 | 10.0 | 20.0 | 30.0 | 40.0 | 50.0 | 60.0 | 70.0 | 80.0 | 90.0 |
|---|---|---|---|---|---|---|---|---|---|---|
| 1.0 | 0.806 | 0.843 | 0.947 | 0.966 | 1.00 | 1.02 | 1.03 | 1.03 | 1.02 | 1.00 |
| 2.0 | 0.788 | 0.906 | 0.947 | 0.941 | 0.945 | 0.949 | 0.953 | 0.989 | 0.991 | 1.00 |
| 3.0 | 0.769 | 0.813 | 0.893 | 0.936 | 1.03 | 0.984 | 0.977 | 1.03 | 1.03 | 1.00 |
| 4.0 | 0.868 | 0.949 | 1.01 | 0.996 | 1.02 | 1.03 | 1.04 | 1.01 | 1.01 | 1.00 |
| 5.0 | 0.831 | 0.931 | 0.994 | 1.03 | 1.07 | 1.05 | 1.03 | 1.01 | 1.02 | 1.00 |
| 6.0 | 0.819 | 0.899 | 0.920 | 0.928 | 0.973 | 0.959 | 0.954 | 0.996 | 0.997 | 1.00 |
| 7.0 | 0.844 | 0.944 | 0.985 | 0.969 | 0.962 | 0.967 | 1.01 | 1.02 | 0.979 | 1.00 |
| 8.0 | 0.824 | 0.932 | 0.926 | 0.958 | 0.970 | 0.982 | 0.970 | 0.983 | 0.994 | 1.00 |
| 9.0 | 0.889 | 0.962 | 0.990 | 0.968 | 0.996 | 0.992 | 1.01 | 1.02 | 0.987 | 1.00 |

Values of fitted parameters and radial dose functions are shown in Table VII and the radial dose functions are shown in Fig. 2. The overall accuracy of the fit was excellent, the mean deviation from the average of measured data was less than 2%.

## C. Anisotropy parameters, $F(r,\theta)$, $\phi_{an}(r)$, and $\bar{\phi}_{an}$

The anisotropy function, $F(r,\theta)$, in a Solid Water medium was calculated from measured two-dimensional dose distributions in Solid Water (Fig. 3) using ICWG methodology and are shown in Fig. 4. Numerical values of the anisotropy functions in polar coordinates are given in Tables VIII to XI.[20] From this data, the anisotropy factors, $\phi_{an}(r)$, were calculated and are given in Table XII. As shown in Table XII, the anisotropy factor, $\phi_{an}(r)$, hardly changes with radial distance. The anisotropy constants, $\bar{\phi}_{an}$, are also given in Table XII.

## D. Point source approximation data

The average dose rate times distance squared for a source with an air kerma strength of 1 U were calculated using the point-source approximation [Eq. (13)] and the recommended parameters are given in Table XIII for distances ranging from 1 to 8 cm. As previously noted the average dose rates at 1 cm are less than the dose rate constants by 3% to 9% depending upon the source. This reduction is due to the anisotropy of dose distributions around the source.

## V. SUMMARY OF RECOMMENDATIONS

We recommend that
(1) The ICWG dose calculation formalism embodied in

TABLE X. Calculated anisotropy function, $F(r,\theta)$, for a [125]I Model 6702 source.

| θ(deg) r(cm) | 0.0 | 10.0 | 20.0 | 30.0 | 40.0 | 50.0 | 60.0 | 70.0 | 80.0 | 90.0 |
|---|---|---|---|---|---|---|---|---|---|---|
| 1.0 | 0.477 | 0.549 | 0.753 | 0.895 | 0.993 | 1.03 | 1.04 | 1.04 | 1.02 | 1.00 |
| 2.0 | 0.528 | 0.656 | 0.766 | 0.832 | 0.924 | 0.945 | 0.939 | 1.02 | 1.02 | 1.00 |
| 3.0 | 0.711 | 0.783 | 0.744 | 0.814 | 0.908 | 0.787 | 0.840 | 1.02 | 1.05 | 1.00 |
| 4.0 | 0.550 | 0.610 | 0.690 | 0.885 | 0.955 | 0.960 | 1.01 | 1.03 | 1.03 | 1.00 |
| 5.0 | 0.697 | 0.719 | 0.822 | 0.964 | 0.981 | 0.990 | 0.980 | 1.00 | 1.05 | 1.00 |
| 6.0 | 0.600 | 0.582 | 0.669 | 0.799 | 0.889 | 0.887 | 0.893 | 0.976 | 1.02 | 1.00 |
| 7.0 | 0.701 | 0.708 | 0.793 | 0.815 | 0.839 | 0.891 | 0.983 | 1.01 | 0.961 | 1.00 |

Eq. (2) and based on the use of air kerma strength should be used for interstitial brachytherapy dosimetry.

(2) Liquid water should be the reference medium for describing dose rate distributions around brachytherapy sources.

(3) The data sets given by Tables IV to XII should be the basis of the dosimetry for ^{125}I, ^{192}Ir, and [103]Pd sources.

(4) Treatment planning software vendors should include a data entry option that allows single-source treatment planning data to be entered in tabular form consistent with the methodology presented in this report.

## VI. DISCUSSION

### A. Choice of dose rate constants

For ^{125}I and ^{192}Ir sources, we had the choice of using measured values of dose rate constants from ICWG[1] or Monte Carlo simulation values from Williamson.[18] We chose to recommend Monte Carlo values because the measured values are for dose to water in a Solid Water medium; this requires a calculated correction factor to convert it to dose to water in a water medium. The Monte Carlo analysis of Williamson[18] had made a detailed comparison of measured and calculated values in a Solid Water medium to validate

TABLE XII. Anisotropy factors, $\phi_{an}(r)$, and anisotropy constants, $\bar{\phi}_{an}$, for interstitial sources.

| Distance, r (cm) | Anisotropy factors, $\phi_{an}(r)$ | | | |
|---|---|---|---|---|
| | [103]Pd | [125]I model 6711 | [125]I model 6702 | [192]Ir |
| 1 | 0.921 | 0.944 | 0.968 | 0.991 |
| 2 | 0.889 | 0.936 | 0.928 | 0.947 |
| 3 | 0.820 | 0.893 | 0.897 | 0.970 |
| 4 | 0.834 | 0.887 | 0.942 | 0.989 |
| 5 | 0.888 | 0.884 | 0.959 | 0.998 |
| 6 | | 0.880 | 0.891 | 0.949 |
| 7 | | 0.901 | 0.907 | 0.965 |
| 8 | | | | 0.955 |
| 9 | | | | 0.974 |
| Anisotropy constants $\bar{\phi}_{an}$ | 0.90 | 0.93 | 0.95 | 0.98 |

TABLE XIII. Average dose rate times distance squared for a source with an air kerma strength of 1 U using the point source approximation.

| Distance along transverse axis (cm) | Dose rate$\times r^2$ (cGy h$^{-1}$ cm$^2$) | | | |
|---|---|---|---|---|
| | $^{103}$Pd | $^{125}$I model 6711 | $^{125}$I model 6702 | $^{192}$Ir |
| 0.5 | 0.857 | 0.848 | 0.915 | 1.09 |
| 1.0 | 0.666 | 0.818 | 0.884 | 1.10 |
| 1.5 | 0.510 | 0.758 | 0.825 | 1.10 |
| 2.0 | 0.383 | 0.681 | 0.752 | 1.11 |
| 2.5 | 0.283 | 0.598 | 0.672 | 1.11 |
| 3.0 | 0.206 | 0.517 | 0.592 | 1.11 |
| 3.5 | 0.150 | 0.443 | 0.518 | 1.11 |
| 4.0 | 0.110 | 0.379 | 0.451 | 1.11 |
| 4.5 | 0.0820 | 0.325 | 0.393 | 1.10 |
| 5.0 | 0.0595 | 0.281 | 0.343 | 1.09 |
| 5.5 | | 0.246 | 0.302 | 1.08 |
| 6.0 | | 0.216 | 0.266 | 1.07 |
| 6.5 | | 0.191 | 0.235 | 1.05 |
| 7.0 | | 0.167 | 0.207 | 1.03 |
| 7.5 | | | | 1.02 |
| 8.0 | | | | 1.00 |
| 8.5 | | | | 0.988 |
| 9.0 | | | | 0.978 |

the accuracy of the simulations. Therefore, the task group recommends the dose rate constants taken directly from the Monte Carlo simulations of Williamson.[18]

The same procedure was not possible for $^{103}$Pd sources because the Monte Carlo simulations of Williamson[18] did not accurately reproduce the measured dose rate constant for $^{103}$Pd sources in a Solid Water medium. For $^{103}$Pd sources we used data from measurements in a Solid Water medium and used a conversion factor calculated by Monte Carlo simulations of Williamson[18] to obtain the dose rate constant in a water medium.

## B. Impact of NIST standards for source strength on the recommended protocol

Of the sources discussed, only $^{192}$Ir has a NIST primary source strength standard that rigorously agrees with the definition of air kerma strength. In the case of $^{125}$I seeds, there is good evidence[18] that the NIST exposure standard established in 1985 was contaminated by nonpenetrating low energy photons. Briefly, the in-air kerma measurements performed by NIST along the transverse axis of sample $^{125}$I seeds were contaminated by 4.5 keV titanium characteristic x rays, which have significant penetration in air but penetrate only $\approx$0.1 mm in condensed matter. The effect of this contamination is to increase the air kerma strength per contained millicurie by 7%–10% without affecting the dose rate in condensed medium at 1 cm. Consequently, the dose rate constant for both the 6702 and 6711 seed models is depressed by 7%–10%. This conclusion is accepted by NIST and it is currently revising the $^{125}$I source strength standard and plan to suppress the contaminant low energy photons. No traceable source strength standard of any type is available for $^{103}$Pd. The vendor calibrates the seeds in terms of activity: however, the accuracy with which the vendor's calibration

procedure realizes the definitions of contained or apparent activity is unknown. Similarly, the accuracy with which the conversion factor in Table IV yields air kerma strength is unknown. Because the physical status of the vendor's calibration is unknown, the average of the two published dose rate measurements at 1 cm was normalized to the vendor's activity calibration to give the dose rate constant.

In the cases of $^{103}$Pd and $^{125}$I, the recommended dosimetry data are based upon a critical comparison of Monte Carlo calculations and measured dose rate distributions.[18] The measured and Monte Carlo dose rate data is normalized to the NIST source strength standard established in 1985. The Monte Carlo calculations include corrections for the low energy contaminant photons included in the standard as described above. The absolute dose rate per unit activity for $^{103}$Pd is based upon an average of the two experimental data sets available as of 1992 and normalized to the vendor-maintained calibration standard in use at that time. The continued accuracy of both the measured and Monte Carlo data require that the vendors consistently apply the calibration procedures and standards current at the time the measurements and calculations were made. An important consequence of this analysis is that when the $^{103}$Pd and $^{125}$I source strength standards are revised, the data in this report will have to be updated. This logical relationship between the source strength standards and accuracy of dose calculations should be kept in mind. Should the standards underlying vendor calibration of these sources change, the dose rate constants recommended by this report must be corrected by the ratio of air kerma strength defined by the old standard to air kerma defined by the new standard for the same seed

$$\Lambda_{new} = \Lambda_{old} \cdot \left[ \frac{S_k \text{ old standard}}{S_k \text{ new standard}} \text{ for the same seed} \right]. \quad (15)$$

The absolute dose rate measurements upon which this report are based utilized LiF thermoluminescent dosimeter (TLD) measurements. As TLD detectors are secondary dosimeters, their sensitivity to dose is determined by measuring their response to a known dose delivered by a calibrated reference beam. Since reference beam calibrations are traceable to NIST $^{60}$Co and x-ray beam air kerma standards, the absolute dose rate measurements endorsed by this report are subject to change should the underlying air kerma standards be revised. This qualification applies only to the $^{103}$Pd dose rate constant value as the Monte Carlo dose rate constant values used for $^{125}$I and $^{192}$Ir do not depend on primary dosimetric standards. Any future revisions of the air kerma standards are expected to be small in relation to the overall uncertainty of the reported measurements.

## C. Uncertainty estimate

The recommended formalism for the dosimetry of interstitial brachytherapy sources requires a knowledge of the following quantities:

air kerma strength, $S_k$
dose rate constant, $\Lambda$
geometry factor, $G(r, \theta)$
anisotropy function, $F(r, \theta)$

radial dose function, $g(r)$.

Air kerma strength is usually provided by the manufacturer for a batch of sources. It is the responsibility of the medical physicist to ensure that actual air kerma strength is in agreement with the manufacturer's values. Uncertainty in the determination of air kerma strength is estimated to be 5%. Dose rate constant, $\Lambda$, also has a measurement uncertainty of about 5%; about 3% in the dose determination and about 3% in the determination of air kerma strength of the sources used in the determination of dose rate constant. The anisotropy function, $F(r, \theta)$ is a ratio of two dose rates each having a measurement uncertainty of about 3%; therefore the uncertainty in its determination is also about 5%. Similarly, radial dose function, $g(r)$, is a ratio of two dose rates, and has a measurement uncertainty of 5%. The geometry factor is a mathematical quantity with minimal uncertainty.

Adding these uncertainties in quadrature, the overall uncertainty in determination of dose rate at a point $(r, \theta)$ around a source using the recommended protocol is estimated to be about 10%.

## D. Implementation of recommended dosimetry protocol

Since use of the dose rate distributions endorsed by this protocol can result in differences of up to 17% in the actual dose delivered to a target volume for some of the brachytherapy sources, it is important that a qualified medical physicist develop a careful plan to implement these recommendations for clinical use. Different commercial treatment planning systems employ different algorithms and require different types of input data. One should clearly understand the specific dose calculation algorithm in one's treatment planning system and then derive the necessary input data from the basic dosimetry parameters provided in this report.

To check the validity of the correct implementation of the recommended protocol, the physicist should calculate the dose rates at various points along the transverse axis using the point-source approximation and compare his/her results with those given in Table XIII.

## E. Clinical impact of recommendations

Appendix C of this report presents an historical review of previous interstitial brachytherapy dose measurements and dose calculation practices. In the perspective of this historical review a dosimetry calculation formalism and the associated numerical data for the dosimetry parameters are recommended. A reduction of the dose rate constants by up to 17% is recommended for ^{125}I sources. No numerical change is necessary for ^{192}Ir sources. The dosimetry assumed by previously published clinical studies using ^{125}I sources needs to be reevaluated in light of recent dosimetry advances upon which this report is based. The purpose of this evaluation is to determine the value of ^{125}I dose rate constants upon which one's current dose prescriptions are based. For example, if dose to full decay in a permanent implant using ^{125}I model 6711 had been prescribed to be 160 Gy using older dosimetry based upon $L = 1.32$ cGy h$^{-1}$ mCi$^{-1}$ (excluding anisotropy), then the actual dose according to the new data would

be $160 \times 0.83 = 139$ Gy. Thus, to deliver the same dose, the physician should prescribe 139 Gy if the new dosimetry is adopted. Adoption of these recommendations will affect the dosimetry of ^{125}I implants by up to 17%; therefore, the medical physicist and radiation oncologist should carefully compare their current dose calculation practice to the recommended protocol. Additionally, they should evaluate the differences between the current protocol and older dosimetry methods assumed by clinical studies cited in support of dose prescription practice.

## F. Impact of recommendations on radiobiological studies

The new dosimetry may also affect values used for the relative biological effectiveness (RBE) of ^{125}I relative to other radionuclides. Changes may be necessary if the biological studies relied upon the old dosimetry parameters to determine the dose to cells and tissues in experiments. On the other hand, if the dosimetry was performed using independent means such as Fricke dosimetry, the RBE values need not change.

It should be noted that the current values of dose rate constant for model 6702 and 6711 ^{125}I seeds are the same (for those who have not adopted the ICWG data presented in Chap. 3)[1] and they differ from the new values by varying amounts, i.e., 10% and 17%, respectively. Therefore, the dosimetry in current use results in a larger dose to the tumor by 7% in the case of 6702 compared to 6711 seeds. This, in effect, can be misinterpreted as an RBE of 1.06. Clearly, it is essential to use the best available values for dosimetry in radiation oncology and biology. Otherwise quantitative conclusions about the relative efficacy and RBEs of different isotopes may not be valid.

## APPENDIX A: RELATIONSHIP OF RECOMMENDED DOSE CALCULATION FORMALISM TO SOURCE STRENGTH QUANTITIES OTHER THAN AIR KERMA STRENGTH

Historically, the strength of sealed brachytherapy sources has been specified using a variety of physical quantities and units. Sources utilizing [226]Ra substitutes, such as ^{137}Cs and ^{192}Ir, have usually been specified in terms of equivalent mass of radium $(M_{eq})$ while the quantity "apparent" or "effective" activity $(A_{app})$ has been used in ^{125}I and [198]Au dosimetry. The TG-43 formalism has been developed around the source strength quantity, air kerma strength, in agreement with the worldwide trend to replace the often bewildering array of historical quantities with a single explicit output quantity defined in terms of SI-compatible quantities and units.[13] Recognizing that the older quantities still retain wide currency in clinical practice, equations relating the dose calculation formalism to these quantities are developed. For a more complete discussion of source strength quantities and units, and more extensive unit conversion tables, the reader is directed to Williamson and Nath.[14] To reduce the length of the equations, the relative dose distribution, $S(r, \theta)$, is defined as follows:

$$S(r,\theta) = \frac{G(r,\theta)}{G(r_0,\theta_0)} F(r,\theta)g(r). \tag{A1}$$

In terms of the distribution $S(r,\theta)$, the absorbed dose rate for sources specified in terms of equivalent mass of radium, apparent activity, and reference exposure rate $(R_x)$ are

$$\dot{D}(r,\theta) = M_{eq}(S_k/M_{eq})\bigwedge S(r,\theta), \tag{A2}$$

$$\dot{D}(r,\theta) = A_{app}(S_k/A_{app})\bigwedge S(r,\theta), \tag{A3}$$

$$\dot{D}(r,\theta) = R_x(S_k/R_x)\bigwedge S(r,\theta). \tag{A4}$$

The conversion factors are given by

$$(S_k/M_{eq}) = (\Gamma_\delta)_{x,\text{Ra},0.5}[W/e], \tag{A5}$$

$$(S_k/A_{app}) = (\Gamma_\delta)_x[W/e], \tag{A6}$$

$$(S_k/R_x) = [W/e], \tag{A7}$$

where $[W/e]$ is the average energy to produce an ion pair in dry air and has the value 33.97 J/C=0.876 cGy/R.[21] $(\Gamma_\delta)_{x,\text{Ra},t}$ is the exposure rate constant for $^{226}$Ra filtered by the thickness, $t$, of platinum and has the value (Ref. 22) 8.25 R cm$^2$ mg$^{-1}$ h$^{-1}$ when $t=0.5$ mm Pt. $(\Gamma_\delta)_x$ is the assumed exposure rate for an unfiltered point source of the given radionuclide and usually has units of R cm$^2$ mCi$^{-1}$ h$^{-1}$. In evaluating Eq. (A6), care must be taken to assume the same $(\Gamma_\delta)_x$ value as assumed by the vendor in calculating $A_{app}$ from the measured $S_k$. Source-strength conversion factors for the sources covered in this report are given in Table IV. Alternatively, the dose rate constants may be renormalized.

$$\dot{D}(r,\theta) = A_{app}\bigwedge_A S(r,\theta), \tag{A8}$$

where

$$\bigwedge_A = (S_k/A_{app})\bigwedge. \tag{A9}$$

The corresponding equations for reference exposure rate and equivalent mass of radium can be easily derived.[14] When equivalent mass of radium is used, the dose rate is given by

$$\dot{D}(r,\theta) = M_{eq}\bigwedge_{M_{eq}} S(r,\theta), \tag{A10}$$

where

$$\bigwedge_{M_{eq}} = (S_k/M_{eq})\bigwedge. \tag{A11}$$

For reference exposure the corresponding equations are

$$\dot{D}(r,\theta) = R_x\bigwedge_R S(r,\theta), \tag{A12}$$

$$\bigwedge_R = (S_k/R_x)\bigwedge. \tag{A13}$$

## APPENDIX B: RELATIONSHIP BETWEEN RECOMMENDED FORMALISM AND OTHER FORMALISMS

An exhaustive review of the great variety of dosimetric ratios used in the brachytherapy dosimetry literature is beyond the scope of this report. A few of the more influential quantities likely to be used by current treatment planning software will be discussed. The purpose of this review is to (i) aid physicists in converting published dose distribution data to the formalism endorsed and (ii) facilitate entry of the recommended data into commercial treatment planning systems not using the TG-43 formalism.

### A. Radial dose distribution quantities

Many quantities have been used to describe the dosimetric interplay between attenuation of primary photons and buildup of scattered photons in the medium. These quantities have been used to describe both theoretical dose distributions around point sources and measurements and/or Monte Carlo calculations around actual sources. In addition, these quantities are used to implement the point-source dose computation model on clinical treatment systems. Radial dose functions derived from the theoretical point-source dose model cannot be related rigorously to the quantities $g(r)$ and $F(r,\theta)$ recommended by this report because the latter are derived from dose distributions around actual two-dimensional sources.

### 1. Energy-absorption buildup factor: $B(\mu r)$

This quantity is generally used to tabulate theoretical point-source dose distributions. The build up factor is defined as

$$B(\mu r) = \left.\frac{\text{total absorbed dose}}{\text{primary absorbed dose}}\right\} \text{ at distance } r \text{ from a point source,} \tag{B1}$$

where $\mu$ is the total linear attenuation coefficient of the primary spectrum. The most commonly cited source of buildup factors is the classic article by Berger[23] which is based upon a semianalytic solution of the Boltzmann transport equation. Burns and Raeside[24] used this formalism to present Monte Carlo estimates of dose rate around $^{125}$I sources. Meisberger *et al.*[25] were the first to suggest that these theoretical data could be used to approximate the transverse axis dose distri-

bution around actual interstitial sources. For an ideal point source, dose rate $\dot{D}(r)$ at distance $r$, air kerma strength, and $B(\mu r)$ are related by

$$\dot{D}(r) = S_k(\overline{\mu_{en}/\rho})^{\text{wat}}_{\text{air}} e^{-\mu r}[B(\mu r)/r^2]. \tag{B2}$$

For a real source, theoretical values of $B(\mu r)$ are approximately related to the actual radial dose function, $g(r)$, by

$$g(r) \simeq e^{-\mu r} B(\mu r)/e^{-\mu r_0} \cdot B(\mu r_0). \tag{B3}$$

This approximation is valid only if filtration and self-absorption do not alter the primary photon spectrum or the balance between buildup of scattered photons and attenuation of primary photons in the transverse plane of the source. That is, the only factor causing the actual dose distribution to deviate from that of a theoretical point source is the spatial distribution of radioactivity in the extended source. This approximation has been confirmed only for lightly filtered sources with photon energies above 300 keV, e.g., ^{137}Cs and [192]Ir. Use of Eq. (B3) for low energy sources such as ^{125}I and [103]Pd is not recommended. Assuming that Eq. (B3) is valid, dose rates very near the source can be estimated by

$$\dot{D}(r,\pi/2) = S_k \overline{(\mu_{en}/\rho)_{air}^{wat}} e^{-\mu r} B(\mu r) G(r,\pi/2). \tag{B4}$$

## 2. Tissue attenuation factor: T(r)

The tissue attenuation factor, $T(r)$, is the most frequently used data format for representing the radial dose falloff around brachytherapy sources in computerized treatment planning systems, which generally request the data in the form of a polynomial fit or a table. $T(r)$ has been used to describe both measured dose distributions[25] around actual sources and theoretical point-source dose distributions.[28] It is defined as

$$T(r) = \left. \begin{array}{c} \dfrac{\dfrac{\text{exposure in water}}{\text{exposure in air}}}{\dfrac{\text{dose in water}}{\text{water kerma in free space}}} \end{array} \right\} \text{ at distance } r \text{ from a point source.} \tag{B5}$$

Experimental determination of $T(r)$ involves direct measurement of both dose in medium and kerma in free space along the transverse axis of an extended source. To satisfy the definition in Eq. (B5), the measured dose and kerma rates must be corrected for finite source size. The most frequently cited $T(r)$ data is that of Meisberger *et al.*,[25] who reviewed both measured and transverse axis dose distributions for ^{192}Ir, ^{137}Cs, [226]Ra, ^{60}Co, and [198]Au and recommended an averaged data set for clinical use.

Regardless of whether kerma-to-dose conversion factors are derived from measured data corrected for source geometry or theoretical point-source calculations, $T(r)$ is related to the radial dose function, $g(r)$, endorsed in this report by

$$g(r) \simeq T(r)/T(r_0). \tag{B6}$$

For measured data, the accuracy of the approximation depends on the adequacy of the experimentalist's source geometry corrections to account for differences in source construction between the source used for measurement and the source to which the data is to be applied. For $T(r)$ data derived from point-source theoretical calculations, the conditions outlined above must be met. For low energy sources, only measured or Monte Carlo data derived from sources of the same design as the actual sources should be used clinically. Subject to these conditions, the dose rate on the transverse axis is given by

$$\dot{D}(r,\pi/2) = S_k \overline{(\mu_{en}/\rho)_{air}^{wat}} T(r) G(r,\pi/2) \tag{B7}$$

## 3. The older (Dale's) radial dose function: g'(r)

The radial dose function, $g'(r)$, is widely used to describe dose distributions measured around actual sources (Ling,[6] Schell,[7] Meigooni[26]), Monte Carlo estimates of dose around two-dimensional sources (Williamson[27]), and theoretical point-source distributions (Dale[15-17]). The symbol $g'(r)$ is

used to denote this quantity so as to distinguish it from the identically named quantity, $g(r)$, endorsed by this report. $g'(r)$ is defined as

$$g'(r) = \dot{D}(r,\theta_0) r^2 / \dot{D}(r_0,\theta_0) r_0^2, \tag{B8}$$

where normally $r_0 = 1$ cm and $\theta_0 = \pi/2$. The function $g'(r)$ is identical to the recommended $g(r)$ except that a point-source geometry distribution is assumed. When $g'(r)$ is derived from measurements or Monte Carlo calculations about an actual source, $g'(r)$ and $g(r)$ are related by

$$g(r) = g'(r)[r_0^2 G(r_0,\theta_0)/r^2 G(r,\theta_0)]. \tag{B9}$$

$g'(r)$ very closely approximates $g(r)$ for distances $r$ greater than the maximum dimension of the active source. However, at distances less than 5 mm from interstitial seeds, the two quantities may differ significantly.

Absolute dose rates cannot be calculated from $g'(r)$ unless the relationship between dose rate at 1 cm and source strength is known. For radium substitute isotopes (energy >300 keV), the dose rate in medium at 1 cm can be closely approximated by the water kerma rate in free space at the same point. Then, assuming $g'(r)$ is based upon measured data

$$\dot{D}(r,\pi/2) = S_k \overline{(\mu_{en}/\rho)_{air}^{wat}} G(r_0,\pi/2)[g'(r)/r^2]. \tag{B10}$$

When $g'(r)$ is used to denote theoretical point-source dose distribution, then, subject to the conditions described above we have

$$g(r) \cong g'(r). \tag{B11}$$

Then dose rate in water medium can be estimated by

$$\dot{D}(r,\pi/2) = S_k \overline{(\mu_{en}/\rho)_{air}^{wat}} g(r) G(r,\pi/2). \tag{B12}$$

## 4. Relationship between dose rate constant and traditional dosimetric quantities

This section reviews the relationships between dose rate constant ($\Lambda$), buildup factor [$B(\mu r_0)$], dose-to-kerma factors [$T(r)$], exposure rate constants ($\Gamma_\delta)_x$, and exposure-to-dose conversions ($f_{med}$). The twofold purpose is to assist physicists in reformatting published data into the recommended formalism and in implementing the recommended dose calculation formalism on treatment planning systems that use traditional quantities. The reader is warned that published values of $B$, $T$, $\Gamma$, and $f_{med}$ derived from idealized point-source calculations ignore essential properties of the actual source including source geometry, encapsulation, and calibration procedures. For low energy sources, such as $^{103}$Pd and $^{125}$I, this approach gives rise to significant errors in dose administered to the patient.

Consider an extended source and assume the transverse axis $T(r)$ and $B(\mu r_0)$ are derived from theoretical point-source calculations. Then the dose rate constant, $\Lambda$, is given by

$$\Lambda = (\overline{\mu_{en}/\rho})_{air}^{wat} T(r_0) G(r_0, \theta_0)$$

$$= (\overline{\mu_{en}/\rho})_{air}^{wat} e^{-\mu r_0} \cdot B(\mu r_0) G(r_0, \theta_0),$$    (B13)

where $\Lambda$ has units of cGy h$^{-1}$ U$^{-1}$ or equivalently, cm$^{-2}$, and $(\overline{\mu_{en}/\rho})_{air}^{wat}$ is the ratio of mass energy absorption coefficients averaged over the primary photon spectrum in free space with respect to energy fluence. In terms of $\Gamma$ and $f_{med}$, the dose rate constants $\Lambda$ and $\Lambda_A$, with units of cGy h$^{-1}$ U$^{-1}$ and cGy mCi$^{-1}$ h$^{-1}$, respectively, are given by

$$\Lambda = (A_{app}/S_k)(\Gamma_\delta)_x f_{med} T(r_0) G(r_0, \theta_0),$$    (B14)

$$\Lambda_A = (\Gamma_\delta)_x f_{med} T(r_0) G(r_0, \theta_0).$$    (B15)

## 5. Implementation of point source model on a commercial treatment planning computer

Treatment planning systems that approximate interstitial seed dose distributions by the isotropic point-source model generally use one of the following equations, which express dose rate as a function of $(\Gamma_\delta)_x$, $f_{med}$, and $T$ or $g'(r)$:

$$\dot{D}(r) = A_{app}(\Gamma_\delta)_x f_{med}[T(r)/r^2],$$

$$\dot{D}(r) = A_{app}(\Gamma_\delta)_x f_{med}[g'(r)/r^2],$$

$$\dot{D}(r) = M_{eq}(\Gamma_\delta)_{x,Ra,0.5} f_{med}[T(r)/r^2],$$    (B16)

$$\dot{D}(r) = M_{eq}(\Gamma_\delta)_x f_{med}[g'(r)/r^2].$$

Using the data and calculation formalism recommended by this report

$$\dot{D}(r) = S_k \Lambda [G(r, \theta_0)/G(r_0, \theta_0)] g(r) \bar{\phi}_{an}.$$    (B17)

Assuming the dose calculation formalism of the planning computer is described by the first equation of (B16) and that the recommended dosimetric data are entered according to the following identifications, Eq. (B17) can be implemented by the following transformations:

$$A_{app} \rightarrow S_k,$$

$$(\Gamma_\delta)_x f_{med} \rightarrow \Lambda \bar{\phi}_{an}/G(r_0, \theta_0),$$    (B18)

$$T(r) \rightarrow r^2 G(r, \theta_0) g(r).$$

## B. Two-dimensional dose distribution and the Sievert integral model

Since every commercial treatment planning system does not permit tabular entry of two-dimensional brachytherapy data, incorporation of the two-dimensional dose distribution data contained in this report may be difficult or impractical for many users. Nearly all currently available treatment planning systems make use of the Sievert model to generate two-dimensional dose rate arrays for filtered line sources. In terms of air kerma strength, the Sievert model is given by[28]

$$\dot{D}(r, \theta) = S_k e^{\mu' t} I(r, \theta, L, t)$$    (B19)

where

$$I(r, \theta, L, t) = \frac{(\overline{\mu_{en}/\rho})_{air}^{wat}}{Lr \cos \theta} \int_{\theta_1}^{\theta_2} e^{-\mu' t \sec \phi} T$$

$$\times [(r \cos \theta - t)\sec \phi] d\phi$$    (B20)

and the other variables are defined by Fig. 1.

The radial thickness of the filter is denoted by $t$ and $\mu'$ is the effective attenuation coefficient of the filter material. Notice that the angle $\theta$ is measured relative to the transverse bisector rather than the longitudinal axis of the source. Equating the general expression (1) for 2-D dose rate distribution with Eq. (B19)

$$\Lambda [G(r, \theta)/G(r_0, \theta_0)] F(r, \theta) g(r) \simeq e^{\mu' t} I(r, \pi - \theta, L, t).$$    (B21)

Duplication of the two-dimensional data recommended by this report by the Sievert model requires that $\mu'$ be treated as a parameter of best fit, chosen to minimize the deviations from Eq. (B21) when the recommended data are used to evaluate the left side. Diffey *et al.*[29] and Williamson[28] have successfully used this approach to "fit" the Sievert model to measured and Monte Carlo-generated dose distributions for $^{137}$Cs intracavitary sources. Because the effect of filtration is assumed to be independent of distance ($\mu'$ is a constant), the Sievert model as described probably cannot accurately model sources for which the scatter-to-total-dose ratio varies significantly with distance. For $^{125}$I, Larke[30] shows that the one-parameter best-fit model of Eq. (B19) gives rise to dose calculation errors as large as 25%.

## APPENDIX C: REVIEW OF DOSIMETRY CALCULATIONS AND MEASUREMENTS FOR INTERSTITIAL BRACHYTHERAPY SOURCES

This section is an historical review of the dosimetry of interstitial brachytherapy sources of $^{192}$Ir (Sec. A), $^{125}$I (Sec. B), and $^{103}$Pd (Sec. C). Because of the extensive amount of literature on this subject in the last two decades, this appendix is rather lengthy. However, the reader is advised that the material presented in this appendix is not essential for using

the recommendations of the task group, but is useful for a better and deeper understanding of the associated issues.

We have decided to present an historical review using the quantities and units that were in use at the time of writing of the specific reports, because it is easier for the reader to relate to the earlier work in terms of its own quantities and units. Also, in this historical review, we have used terms like excellent agreement, good agreement, and fair/reasonable agreement to be roughly equivalent to an agreement within 3%, 5%, and 10%, respectively.

## A. Iridium-192 sources

*1966*: Among the earliest reported dosimetry data for $^{192}$Ir were those of Meredith *et al.*,[31] who had used a cylindrical perspex ion chamber (6 mm×6 mm internal dimensions) to measure exposure in air and in water separately at 1 or 2 cm intervals in the range 2–10 cm from a 1.5 cm long $^{192}$Ir source. At each distance they formed the ratio of exposure in water to exposure in air from measurement data uncorrected for source size or detector size, acknowledging that such corrections are not exactly the same in water as in air. The resulting ratios were within experimental uncertainty (about 2.5%) equal to 1.0 from 2–6 cm, dropping to 0.94 at 8 cm and 0.90 at 10 cm.

*1968*: Meisberger *et al.*[25] measured the water/air ratio (without moving the detector) at distances from 1 to 10 cm from a cluster of seeds (3 mm length×0.5 mm diameter each, steel walls 0.2 mm) using a 3 mm×3 mm anthracene scintillator with a Lucite light pipe to a photomultiplier. They mention making source size corrections but did not say how they were made. They also calculated the ratio of exposure in water to exposure in air, using (as yet unpublished) Berger buildup coefficients. The calculated results diverged from the measured for increasing distance and were about 7% larger than measured data at 10 cm. They averaged their data with those of Meredith *et al.*[31] and then further averaged the combined experimental data with their calculated data. The resulting curve was fitted with a third degree polynomial for which the constant term was 1.01 (versus an expected value of 1.00) and the value at 10 cm was about 0.93. They recommended this curve for clinical calculations.

*1979*: Because dose estimates are often made on the basis of exposure calculated from activity, the exposure rate constant has continued to be a matter of interest, although it will be of much less interest when source strengths are routinely specified as air kerma strength. Prior to 1978, exposure rate constants reported for $^{192}$Ir ranged from 3.9 to 5.0 R cm$^2$ mCi$^{-1}$ h$^{-1}$, providing a good example of why it is poor practice to specify source strength as activity, since the activity might be inferred by the manufacturer using one value of the constant and the dose might be calculated by the user from a different value. Glasgow and Dillman[3] attempted to reconcile the disparate values of exposure rate constants and reported their own calculated value, 4.69±0.05 R cm$^2$ mCi$^{-1}$ h$^{-1}$, based on the then latest spectroscopy data from the Evaluated Nuclear Structure Data File at Oak Ridge National Laboratory. Although, strictly speaking, the exposure rate constant is defined (except in the case of radium) only for an unencapsulated point source, Glasgow[32] subse-

quently used the same nuclear data to calculate exposure rate constants for two types of $^{192}$Ir sources: one encapsulated in stainless steel and the other in platinum. These results would allow one to estimate the actual activity in a source from a measurement of exposure rate but have no practical application in brachytherapy dosimetry.

*1979*: Webb and Fox[33] used Monte Carlo methods to calculate the dose rate as a function of distance from an unencapsulated point source of $^{192}$Ir at the center of a 25 cm radius water sphere. Their value at 1 cm, 4.26 cGy h$^{-1}$ mCi$^{-1}$, cannot conveniently be referenced to a source strength given in terms of exposure rate, since they did not report using the same code to calculate exposure rate. However, they did present results normalized at 1 cm and noted that "if the data in Fig. 4 of Meisberger *et al.*[25] can be interpreted as representing the radial falloff in dose rate with the inverse square law removed," their results duplicated almost exactly Meisberger's "selected average" of experimental and calculated data. It is not clear that, in making this comparison, the authors have taken into account the fact that Meisberger's plot was inherently normalized at zero distance while Webb and Fox data were normalized at 1.0 cm; Meisberger's polynomial, if normalized at 1.0 cm, gives 0.910 at 10 cm, whereas Webb and Fox's normalized data have a value of about 0.945 at 10 cm. In a short note two years later, Kornelsen and Young[34] suggested that the data of Webb and Fox[33] could be represented by $e^{-\mu r}B/r^2$ where $\mu$ is a linear attenuation coefficient and $B$ is a buildup factor of the form

$$B = 1 + k_a(\mu r)^{k_b}$$

and $k_a$ and $k_b$ are constants. With a value of 0.113 cm$^{-1}$ for $\mu$, least-squares fitting resulted in $k_a = 1.59$ and $k_b = 1.36$ for the $^{192}$Ir data.

*1981*: Boyer *et al.*[35] have measured exposure rate constants for the 0.2 mm stainless steel-clad and the 0.1 mm platinum clad $^{192}$Ir source to be 4.6 R cm$^2$ h$^{-1}$ mCi$^{-1}$ with a 4% uncertainty. By offering calibrations of brachytherapy sources only in terms of exposure rate at a given distance, NIST has exerted a positive influence toward avoiding errors associated with uncertainties in exposure rate constant. Having introduced a calibration procedure for $^{137}$Cs intracavitary sources in 1969, the National Bureau of Standards (NBS) subsequently reported a similar methodology for the calibration of $^{192}$Ir seeds.[36] Spherical air filled graphite chambers were used to measure the exposure rate at either 50 or 100 cm from planar arrays of closely spaced seeds, either platinum encapsulated or stainless-steel encapsulated. About 50 seeds of nominal activity 1.5 mCi each were required in an array in order to produce a satisfactory ion current in the (nominally 50 cc) chamber. The seeds were then placed individually at the center of a re-entrant air filled spherical ion chamber having aluminum walls of 20.3 cm diameter, and its calibration factor for each seed type was determined as the ratio of the product of dose and distance squared for the array to the sum of the measured ion currents for the seeds. This factor was 3% higher for the platinum encapsulated seed than for the stainless-steel-encapsulated seed.

It should be noted that Rogers pointed out at a symposium at NIST that for $^{192}$Ir, a small ($\leq 2\%$) discrepancy may exist

between the free-air chamber and cavity chamber standards at intermediate energy photons. Attix made similar comments. The NRC and NIST are investigating the issue.

*1982*: The following year, in an article describing Monte Carlo calculations of dose rate versus distance for point sources of several radionuclides, including ^{125}I as well as ^{192}Ir, in water and other body tissues, Dale[15] pointed out that the sampling method used by Webb and Fox[33] did not accurately represent the actual distribution of scattering events on scattering angle, especially at low energies. [192]Ir photon energies are sufficiently high so that only minor differences among tissues were noted in the calculated dose rate constant (SDC in Dale's terminology), which ranged from 3.96 $cGy\,h^{-1}\,mCi^{-1}$ in rectum to 4.13 $cGy\,h^{-1}\,mCi^{-1}$ in body fat. Similarly, the radial dose functions show only a few percent variation with tissue type. The radial dose function reported by Dale[15] for ^{192}Ir in water is about 0.98 at 10 cm, significantly higher than the corresponding values of either Webb and Fox[33] or Meisberger.[25] The decay scheme used by Dale in these calculations was challenged in a letter to the editor from Mayles and Turner,[37] who suggested that the correct decay scheme would lead to SDC values higher by a factor of 1.089. In a later publication dealing with the same issues, Dale[16] adjusted the SDC values by a factor of 1.09 but did not change the coefficients of the quadratic function that had previously been the result of a least-squares fit to the Monte Carlo calculated radial dose function. Presumably, an increase in the dose rate constant would be accompanied by a more rapid falloff in the radial dose function, which might bring his results into better agreement with the Webb and Fox[33] data and the Meisberger[25] data. In this same article, Dale observed that, for medium-energy nuclides like ^{192}Ir, the average spectral photon energy falls off significantly with distance, to about 60% at 10 cm. He also shows the percentage of dose due to scattered photons, which is still increasing at 15 cm, where it reaches a value in water of about 76% (possibly still based on calculation with the incorrect decay scheme, however).

*1983*: For ^{192}Ir seeds or wire encapsulated in platinum, oblique filtration has a significant effect on the dose near the source. An example of how the Sievert integral is used to estimate this effect in clinical dose calculations for ^{192}Ir wire is afforded in an article by Welsh *et al.*[38] dealing with how their 1966 algorithm (at Churchill Hospital, Oxford) was reevaluated in 1981. Pertinent to the dosimetry of such sources is their decision to retain 4.3 $cm^{-1}$ as the attenuation coefficient for ^{192}Ir photons in platinum and their model of the actual source as a line source on the axis of a cylinder of platinum. For the two wire diameters in use, 0.3 and 0.6 mm, the corresponding products of radius and attenuation coefficient are 0.0645 and 0.129. Of possible relevance, as well, is their choice of attenuation coefficient; for the most extreme case shown, 8 cm distance on the transverse axis of a 10 cm wire, the effect of the choice of attenuation coefficient was less than 6%.

*1983*: It was pointed out by Williamson *et al.*[39] that Sievert integral calculations (such as the aforementioned) implicitly assume any photons scattered by the source capsule are attenuated by the same factor as the unattenuated

primary photons. He reports the results of Monte Carlo calculations (of exposure rate in air) to determine how much error is involved in these assumptions. For a platinum filtered ^{192}Ir seed (0.5 mm diameter and 3 mm long), he found that for angles greater than 50 deg relative to the source axis, the agreement of Monte Carlo with Sievert integral was within 2%; within a cone of less than 50 deg, the Sievert integral overestimates the dose in air by up to 16.6% at 2 cm on the seed axis. He used the same data to depict the (fluence or exposure) anisotropy of the platinum seed, obtaining a ratio between doses on the longitudinal axis and transverse axis of 0.60 by Monte Carlo versus 0.70 by Sievert integral. The Monte Carlo result shows that a point source calculation would be in error by 5% at an angle of 50° from the source axis. Integrated over $4\pi$, the anisotropy produces a reduction in "effective activity" of 4% by Monte Carlo, 2.9% by Sievert integral. The error made by using the Sievert integral is reduced slightly for an ^{192}Ir seed if exposure rate (rather than activity) calibration is used. Finally, Williamson demonstrates that the calculated anisotropy corrections are insensitive to uncertainties in the underlying spectroscopic data when seed strength is specified by exposure rate rather than activity.

*1983*: Ling *et al.*[40] have determined that there is some anisotropy in photon emission associated even with the stainless-steel ^{192}Ir seed. They had used a 3 in. diameter sodium iodide crystal 90–150 cm from a seed (in lightweight mounting) to measure, for four seeds, the relative 250–750 keV photon fluence as a function of angle in the plane of the seed axis. Although the fluence on the axis was found to be only 78% of that on the transverse axis, the value was greater than 95% at 20° from the axis. The average over $4\pi$ solid angle was only 1% different from unity, and they concluded that the observed anisotropy was not significant clinically.

*1985*: Kneschaurek and Lindner[41] used a small ionization chamber (0.3 cc PTW) to measure separately dose in air and dose in polystyrene as a function of distance from 2–10 cm along the transverse axis of a Gamma Med remote afterloader ^{192}Ir source 1 mm in diameter and 2 mm long. They fitted Meisberger polynomial coefficients for the water/air exposure ratio to the polystyrene/air dose ratio, obtaining an attenuation curve that, relative to the Meisberger "selected" water/air ratio, was 1% lower at 2.0 and 3.6% lower at 10 cm.

*1988*: A similar, though more extensive, study of ^{192}Ir photon attenuation in phantom was undertaken by Meli, Meigooni, and Nath *et al.*[42] for Lucite, Solid Water, and water, in addition to polystyrene. They used a Gamma Med source of active dimensions 0.6 mm diameter by 5.5 mm long and made measurements on the transverse axis at distances from 1–10 cm with a 0.1 cc (Physikalisch Technische Bundesanstalt, PTW) ion chamber. They also performed Monte Carlo calculations of dose versus distance from a point ^{192}Ir source in these materials and of spectral distribution on photon energy at various distances from both a bare and a 0.1 mm stainless-steel-encapsulated source, using the updated source spectrum that Mayles and Turner[37] had earlier recommended to Dale.[15] In the calculated spectral results, no effect of encapsulation was seen, and the expected shift toward low en-

ergies at greater distances was observed, more so for Lucite, which is denser. For all the materials, the $f$ factor derived from the calculated spectra decreased by 3% from 1 to 5 cm and held constant at 10 cm. Relative depth versus distance data were within uncertainty limits for both measurements and calculations for all materials, and the water/air dose ratio agreed with Meisberger's selected values within 1.5%. The authors concluded that the solid phantom materials investigated, including Lucite (for which increased absorption was compensated by backscattering in full phantom), were all suitable substitutes for water in experimental measurements.

*1988*: In an article related to the above studies, Meigooni, Meli, and Nath *et al.*[43] determined the effect of spectral change with distance on the sensitivity (thermoluminescent response per unit dose) of LiF (TLD) chips. Using the same ^{192}Ir source and the polystyrene phantom, they placed five chips on the perimeter of a 1.5 cm radius circle within a phantom slab, together with a 0.3 cc PTW ion chamber at the center of the circle. The flat energy response of the chamber was verified experimentally with 60, 80, 100, and 250 keV and 4 MV x rays to be within 2% over the energy spectrum of ^{192}Ir photons. Other slabs were used to vary the phantom thickness between the plane of the detector array and the source, although the total intervening space included a 10 cm air gap adjacent to the phantom surface in which the source was embedded. The air gap served to make negligible the difference in distance from the source between the TLD centers and the chamber center. Introducing the air gap was found to change the ratio of TLD response to chamber response at 10 cm depth in phantom by no more than the 1.7% that would have been expected from the different geometry if responses varied as the inverse square of distance to the source, indicating no significant effect of the gap on photon spectrum. The relative sensitivity of the TLD's was measured at five phantom depths (1.36, 3.34, 5.32, 7.27, and 10.27 cm) and also calculated using Monte Carlo simulations at three (1.0, 5.0, and 10.0 cm). Calculations were performed by weighing sensitivities taken from an experimentally determined response versus energy curve by the Monte Carlo calculated spectra at these depths. Measurements and calculations taken together indicate that the LiF sensitivity increases roughly linearly with depth up to about 8% at 10 cm depth.

*1988*: Gillin *et al.*[44] have reported TLD measurements in Solid Water phantom with LiF cubes 1 mm on an edge, in the vicinity of a platinum encapsulated ^{192}Ir wire 0.3 mm in diameter and 5 cm away from the wire and to 4 cm (from center) along the wire, plus a few points on the source axis, to 4.5 cm from center. They compare their results with calculations that employed a variation of the Sievert integral method and Meisberger scattering and attenuation corrections. Calculated data are substantially smaller than measured data at 0.25 and 0.5 cm away but there is good agreement at greater distances. As expected, the Sievert integral severely underestimates observed doses along the axis, since it does not account for dose from radiation scattered in the phantom. The fact that the calculated values are smaller than measured values at 0.25 and 0.5 cm is probably attributable to the same effect. The effect of scattering in the phantom on the accuracy of the Sievert integral method is thus opposite

to the effect of scattering in the source as determined by Williamson.[39] Since the Sievert integral method starts from actual rather than apparent activity, multiplication of the exposure rate constant by the factor 1.07, in this instance, was required to correct for self-absorption during the exposure rate calibration of the source.

*1988*: In an investigation of the use of platinum encapsulated ^{192}Ir seeds (3 mm diameter by 0.5 mm long) in eye plaques, Luxton *et al.*[45] performed TLD measurements at 22 locations in the region 1.9–10.2 mm from the axis and 0–12 mm along the axis of a single seed in acrylic phantom, using LiF cylindrical rods 1 mm in diameter and 3 mm long. Measurements were found to agree (within 95% confidence limits) with calculations, based upon the isotropic point-source model modified by the line geometry function, everywhere except for the point at 1.9 mm from and 12 mm along the seed axis, where the measured dose was 9.5% greater if angular anisotropy based on the Sievert integral was used in the calculation and 22% greater if Monte Carlo-based anisotropy was assumed, using data from Williamson *et al.*[39] in both cases. Calculation and measurement were also compared along the axis of a gold plaque incorporating four radially placed ^{192}Ir seeds and mounted on an epoxy-resin hemispherical eye phantom, which was in turn affixed to an acrylic block. These data also showed agreement within the 95% confidence limits of the measurements and indicated, further, no significant difference between the axial dose distribution seen with or without the gold plaque in place.

*1989*: TLD measurements along the transverse axis were performed for both platinum and stainless-steel encapsulated ^{192}Ir seeds by Thomason and Higgins,[46] using LiF rods 1 mm×1 mm×6 mm. With the rods' long dimension perpendicular to the transverse axis, data were taken from 1 to 12 cm from the seed center in a Solid Water slab immersed in water. Tabulated correction factors applied to near-source data are identified as the ratio of the average dose over the detector volume to the dose at the center of the detector, although the factors given are greater than 1 (e.g., 1.028 at 1 cm). Results are presented in the form of a relative dose factor (RDF), defined as the product of distance squared and the ratio of measured dose to dose in air at 1 cm, with dose in air at 1 cm having been obtained from the effective exposure rate constants calculated by Glasgow.[32] The possible need to correct for an increasing LiF sensitivity with distance was evaluated by convolving Monte Carlo-calculated spectra (Meli *et al.*[47]) at 1, 5, and 10 cm distances in a phantom with LiF energy absorption coefficients and stopping power ratios to water; since the energy dependence found was less than 1%, no correction was made. The RDF's were compared to the water/air exposure ratio of Meisberger *et al.*[25] and to the RDF of Dale,[15] whose data were normalized at 1.0 cm. For both seed types, the RDF's from this work were 2%–3% less than 1.0 at 1 cm, increased to 1.0 at 3–4 cm and gradually decreased to 0.96–0.97 at 12 cm, a relative variation very close to that of Dale's Monte Carlo point-source data, which had been obtained with an incorrect spectrum. The Meisberger selected data, on the other hand, held constant at about 1.02 at 1–3 cm and then fell off gradually to 0.925 at 10 cm. For both the Meisberger data and the data from this

work, there is an implied normalization to 1.0 at the source center, where point-source doses in water and in air approach equality. If such normalization is taken into account, the RDF here would seem to have an unlikely variation with distance, first decreasing, then increasing and finally decreasing again. The dose rate constants in water inferred from this article are 4.0 cGy h$^{-1}$ mCi$^{-1}$ and 4.2 cGy h$^{-1}$ mCi$^{-1}$, respectively, for the platinum and stainless-steel seeds.

*1989*: The issues of comparing with Dale's differently defined RDF and LiF sensitivity variation with depth in the above article were raised in a letter to the editor from Meli *et al.*[47] In a juxtaposed response, Thomason and Higgins[46] cite as yet unpublished Monte Carlo dose versus distance data that do agree with their uncorrected measured data and suggest that the air gap in the measurements of Meigooni *et al.*[43] may have artificially hardened the $^{192}$Ir spectrum at shallow depths to produce the observed sensitivity variation and that Meigooni's Monte Carlo calculations omitted photons below 200 keV, which make up 7.8% of the primary spectrum. The omission of these photons may have also hardened the shallow-depth spectrum.

*1989*: Weaver *et al.*[8] have reported transverse-axis TLD measurements in Solid Water phantom at distances 0.5–8 cm from a stainless-steel encapsulated $^{192}$Ir seed, using LiF powder calibrated in a $^{60}$Co beam. On the basis of EGS4 Monte Carlo calculations of photon spectrum at depth, together with the mass absorption coefficient relative to water, a correction factor was determined to account for increasing sensitivity of LiF with depth; this factor was 0.95 at 8 cm. A "dose factor" of 4.55±0.07 cGy cm$^2$ mCi$^{-1}$ h$^{-1}$ was found. Since the dose factor as defined is equal to the dose rate constant divided by the (3 mm line source) geometry factor at 1 cm, the corresponding value of the dose rate constant is (0.9926) (4.55)=4.52 cGy mCi$^{-1}$ h$^{-1}$. The authors compare their dose factor with the analogous value for a point source in air, i.e., the product of the *f* factor (0.973 cGy/R) and the exposure rate constant (4.69 R cm$^2$ mCi$^{-1}$ h$^{-1}$), which is 4.56 cGy mCi$^{-1}$ h$^{-1}$. The radial dose factor, which, because it incorporates the line source geometry factor in the denominator [incorrectly shown in Eq. (6) of this article], should approximate the product of normalized dose and distance squared for a point source. This factor was seen by these authors to be 0.98 at 0.5 cm, 0.97 at 5 cm, and 0.86 at 8 cm with estimated uncertainties of 1%–2%. In contrast, Meisberger's polynomial fit (normalized to 1.0 at 1 cm) gives 0.99 at 5 and 0.95 at 8 cm.

*1990*: Another set of measurements of the transverse-axis dose rate in Solid Water phantom for the stainless-steel encapsulated $^{192}$Ir seed was that of Nath, Meigooni, and Meli,[9] who used LiF chips calibrated in air, with an $^{192}$Ir source, against an NBS-calibrated Spokas ion chamber. They applied the depth dependent LiF sensitivity correction determined earlier by Meigooni *et al.*[43] obtained with the high-strength remote afterloader source, and with the Integrated Tigers Series (ITS) Monte Carlo calculation results also reported in this article. Their radial dose function for the $^{192}$Ir source is in good agreement (within 2%) with their own Monte Carlo calculated values, and with both their earlier data[42] for high activity $^{192}$Ir sources of a remote afterloader and recom-

mended values by Meisberger *et al.*[25] They, however, report a significant discrepancy between their values for the radial dose function and Dale's,[15] whose Monte Carlo calculated values for $^{192}$Ir are consistently higher than other data by about 10% at a distance of 10 cm.

*1990*: Similar to the $^{125}$I data, the ICWG also recommended a new set of values for the dose rate constant and radial dose function for the stainless steel-class $^{192}$Ir source (Chap. 3).[1] This data set was an average of the data obtained by the three participating institutions. Unlike the case of $^{125}$I data, the ICWG found that the dose rate constant of 4.55 cGy mCi$^{-1}$ h$^{-1}$ for $^{192}$Ir was in agreement (within 2%) with values in current use. The radial dose function was obtained similarly by averaging the three data sets and was found to be in reasonable agreement (within 2%) with Meisberger's data.[25] As before, the anisotropy constant was found to be 1.00 within experimental uncertainty of ±3%.

*1991*: Recently, Thomason *et al.*[48] have reported a measurement of dose distributions in water using LiF thermoluminescent dosimeters for $^{192}$Ir seed sources with stainless steel and with platinum encapsulation to determine the effect of differing encapsulation. In addition, dose distributions surrounding these sources have been calculated using the EGS4 Monte Carlo code and have been compared to the measured data. The two methods are in good agreement (within 2.5%). Tables are given which describe the dose distribution surrounding each source as a function of distance and angle. In addition, specific dose constants have been determined from results of Monte Carlo simulation. This work has confirmed the utility of the EGS4 Monte Carlo code in modeling $^{192}$Ir seed sources to obtain brachytherapy dose distributions. In an accompanying article, Thomason *et al.*[49] also present an investigation of the effect of source encapsulation on the energy spectra of $^{192}$Ir sources, both with stainless steel and with platinum encapsulation using Monte Carlo simulation. The fractional scatter dose around these sources has also been determined from Monte Carlo simulation. The platinum-encapsulated $^{192}$Ir source exhibited greater attenuation of the primary spectrum and, consistent with this greater attenuation, exhibited more scattered radiation.

## B. Iodine-125 sources

Because of the relatively low energy of $^{125}$I photons, significant absorption occurs in the titanium encapsulation of interstitial seeds, especially in the end welds, and in any x-ray marker contained in the capsule. This absorption, together with the unavoidable position uncertainty associated with markers and with the $^{125}$I-bearing resin beads, has made difficult both calculations and measurements of the dose distribution in water at distances closer than 1 cm to the seed. It is not surprising, therefore, that earlier dose determinations were often normalized to the value of dose rate per unit activity at 1 cm on the transverse axis. The "activity" referenced in this quantity was the activity of an unencapsulated point source that would result in the transverse-axis exposure rate actually measured for the seed at a distance large enough for the inverse square law to be valid.

*1960s*: An historical review of $^{125}$I dosimetry indicates that dose rate data for this isotope has undergone a nearly

factor-of-2 revision since its introduction in the late 1960s. Some of the early dose rate distributions were derived from the simple dose calculation formalism that is suitable only for higher energy photon emitters. For radium and radium substitutes, absorption of primary photons by the medium and buildup of scatter photons almost exactly compensate for one another for distances up to about 10 cm, allowing dose rate per mCi at 1 cm on the transverse axis to be approximated by the product of the exposure rate constant and the exposure-to-dose conversion factor (the $f$ factor). However, it is now known that for $^{125}$I photons this model significantly overestimates absorbed dose even at 1 cm, since buildup of scatter photons fails to compensate for photon attenuation at 1 cm. Secondly, $^{125}$I calibration standards have been revised several times and only in 1985 was a NIST primary standard developed that was based upon exposure.[5] Only when calibration is based upon a well-defined quantity, such as reference exposure rate or air kerma strength, can dose rates derived from Monte Carlo calculations and other theoretical methods be properly normalized. A third reason for the large investigator-to-investigator variability in measured dose rates is the wide variety of phantom materials used in the experiments, including mix-D, Lucite, liquid water, and Solid Water. It is now known that because of dominance of photoelectric effect at low photon energies, even small variations in atomic number of the measurements medium can lead to significant changes in apparent penetration of $^{125}$I photons.

*1972*: The expectation of a buildup-related peak may have been fostered by calculations performed by Loevinger of the ratio of dose in water to exposure in air as a function of distance from a point source of monoenergetic photons.[50] These calculations, which were based on buildup factors calculated by Berger,[23] showed increasingly more prominent and more distant buildup peaks as photon energy increased from 30 to 80 keV. The curve for 30 keV peaked at about 1 cm and an additional curve for 20 keV showed only exponential attenuation (with no peak). It was reasonable to suppose that a comparable plot for $^{125}$I photons, with an average energy of 28.5 keV, might peak at a distance less than 1 cm.

*1975*: The earliest measurements of the $^{125}$I seed dose distribution were those conducted by Holt using lithium fluoride (LiF) (Teflon) thermoluminescent dosimeters (TLD's) in mix-D phantom.[51] The TLD rods, each parallel to the source, were arranged, with their centers in the central transverse plane of the source, in two spirals extending from 0.2 to 4.0 cm from source center. At that time, the source (now called the model 6701) used the same encapsulation as current seed models, but inside the capsule there was a central gold marker ball that separated two radioactive resin beads. The apparent activity (in mCi) was deduced from an exposure rate constant calculated to be 1.4 R cm$^2$ mCi$^{-1}$ h$^{-1}$. The relative dose rate versus distance data, normalized to 1 cm, were fitted by a sum of exponentials and integrated over all space. The dose rate per unit activity at 1 cm was then determined as the factor by which the integral must be multiplied to yield a product equal to a total power output of 8640 erg mCi$^{-1}$ h$^{-1}$, corresponding to a photon energy output of 40.47 keV per disintegration. The factor so determined, 1.68 rad mCi$^{-1}$ h$^{-1}$, was rounded to 1.7 rad mCi$^{-1}$ h$^{-1}$ and incor-

porated, multiplied by the relative data, in a computer lookup table for use in clinical dose calculations at Memorial Hospital. Although the reasons why this determination of the dose rate constant produced such a high value remain obscure, one may note that, taken together with an exposure rate constant of 1.4 R cm$^2$ mCi$^{-1}$ h$^{-1}$, this work implied a very large buildup peak.

*1975*: It was soon recognized[52] at Memorial Hospital that Holt's early data were unrealistic, and a point-source calculation based on absorbed fraction data by Berger produced a curve of distance squared times dose rate with a maximum value of only 1.3 rad cm$^2$ mCi$^{-1}$ h$^{-1}$ at a distance of about 0.7 cm. Subsequent $^{125}$I seed measurements using a hemispherical ion chamber of conductive tissue equivalent plastic led ultimately to a reported value at 1 cm of 1.03 rad cm$^2$ mCi$^{-1}$ h$^{-1}$ for distance squared times dose rate averaged (inherently, in the measurement) over $4\pi$ solid angle.[53] Also reported was a transverse axis value at 1 cm, as a result of TLD measurements in the same tissue equivalent plastic, of 1.18 rad cm$^2$ mCi$^{-1}$ h$^{-1}$, with an implied anisotropy factor of 0.87.[54] These values would have been about 4% lower had they been corrected to water.

*1978*: Dose measurements and calculations for the model 6701 seed were also performed by Krishnaswamy.[55] He used 1 mm by 6 mm lithium fluoride (Teflon) TLD's to measure dose at 1 cm intervals along the transverse axis and at selected other points within a distance of 5 cm in a polymethylmethacrylate (PMMA) phantom. These measurements, together with relative dose measurements using photographic film, were used to supplement point-source calculations based on buildup factors by Berger[23] and compose a two-dimensional table of dose to muscle tissue, extending to 5 cm in both axial and transverse directions in one quadrant of a plane through the seed axis. The calculated value of distance squared times dose at 1 cm on the transverse axis was 1.32 rad cm$^2$ mCi$^{-1}$ h$^{-1}$ and the measured value was only 2% higher. The author pointed out that his relative (normalized to 1 cm) dose values on the transverse axis agreed to within 10% with those by Holt.

*1979*: The angular distribution of photon fluence in air from model 6701 $^{125}$I seeds was measured by Ling *et al.*[56] for each of the three most abundant spectral lines, using a lithium-drifted silicon detector 5 mm thick.[57] For the 27.4 keV photon energy (the most abundant line), the fluence along the seed axis was only 15% of the fluence along the transverse axis. The fluence averaged over $4\pi$ was found to be 14% less than on the transverse axis. A worst case analysis of the effect of this anisotropy on dose distribution in idealized implants, using a two-dimensional lookup table that assumed the same anisotropy in tissue as in air, suggested using treatment margins tighter by 2–3 mm in the direction of seed axes.

*1980*: A further assessment of the effect of $^{125}$I seed photon emission anisotropy was found in another determination at Yale.[58] Using a sodium iodine scintillation detector to measure the photon emission rate from the (model 6701) seed, these investigators found a $4\pi$ average exposure rate constant of 1.089 R cm$^2$ mCi$^{-1}$ h$^{-1}$ on the transverse axis. They compared the latter value to a calculated 1.284

R cm² mCi⁻¹ h⁻¹ transverse axis value of the exposure rate constant with respect to the contained activity in the seed. An anisotropy factor of 0.83 is implied by the measured values.

*1982–86:* Early Monte Carlo dose calculations involving $^{125}$I were those reported by Dale.[15] He evaluated dose as a function of distance (1 to 15 cm data shown) from a point source in water and various body tissues. In particular, he found the dose rate per unit activity at 1 cm in water (a quantity called the "specific dose constant" or SDC) to be 1.35 rad cm² mCi⁻¹ h⁻¹ and he mentions that this result agrees closely with the value obtained experimentally by Krishnaswamy[55] for an actual seed. Monte Carlo values of the specific dose constant for adipose tissue and body fat were 66% and 54%, respectively, of the value of SDC for water. In his data for water, the relative dose rate normalized to the value at 1.0 cm (a quantity called the "radial dose function" or RDF) drops to 0.32 at 6.0 cm, whereas the comparable figure from Ling's data is 0.28. In a subsequent communication in 1983, Dale[16] emphasizes the dependence on tissue effective atomic number of both the SDC and the RDF, i.e., lower-Z tissues have lower SDC's but their RDF's decrease less rapidly with distance. He points out that the $^{125}$I integral dose within a specified radius increases little beyond 10 cm for water but continues its rise (proportional to distance) to about 15 cm for adipose tissue. His Monte Carlo-derived spectral histograms show minimal change with distance for $^{125}$I, with a maximum decrease (at 5 cm) in mean spectral energy of only about 2%; the mean spectral energy of $^{198}$Au, for comparison, has decreased at 10 cm to less than 60% of its original value. Further, the dose contribution of scattered radiation becomes important much closer to the source for $^{125}$I than for higher energy radionuclides, e.g., contributing 50% at 1.8 cm for $^{125}$I as opposed to 6.4 cm for $^{198}$Au. In a further communication 1986, Dale[17] offers revised coefficients for the polynomial fit to his data; with the revised coefficients, the RDF at 6 cm in water is still higher, about 0.37. Other early Monte Carlo studies of $^{125}$I were those of Burns and Raeside,[24] who calculated specific absorbed fractions as a function of distance from a point source in water for individual photon energies. Their values were 2% and 1% higher, respectively, for 27.4 keV and for all other energies than values calculated from data by Berger.[23] Burns and Raeside later expanded[59] this study to calculations for not only point sources but 6701 and 6702 seeds, as well, evaluating dose at 56 points extending from 0.5 to 5 cm radially from the seed axis and from the 0–5 cm in the axial direction. Their point-source dose data in relation to those of Dale[15–17] were 3% lower at 1 cm and 10% lower at 5 cm. They found that the relative dose distribution decreases more rapidly with distance for model 6711 compared to the model 6702 source. To make the latter comparison, they multiplied Krishnaswamy's results by 1.19, the ratio (from their work) of the dose at 1 cm on the transverse axis of a model 6701 seed having the same contained activity. Defined this way, "apparent activity" would appear to differ from the conventionally defined apparent activity by the ratio, at 1 cm on the transverse axis, of dose to the product of exposure and the $f$ factor; it would have the effect of making their results larger by that ratio.

*1983:* Shortly after the introduction of the model 6711 seed in 1983, its dose distribution characteristics were compared with those of model 6701 by Ling *et al.*[60] The photon spectrum from the newer seeds, observed with an intrinsic germanium detector, was found to contain a significant component of silver fluorescence x ray (22.1 and 25.2 keV). Calculations by the Berger method were performed using the newly measured spectrum for a line source model of the model 6711 and the previously measured spectrum for a two point model of the model 6701. Also, a silicon diode detector was used to measure relative dose distribution along the transverse axis for each type of seed at distances from 0.3 to 6.0 cm. Both calculated and measured data were normalized, at a distance of 1.0 cm, to 1.14 rad cm² mCi⁻¹ h⁻¹, a value obtained as the product of the exposure rate constant (1.45 R cm² mCi⁻¹ h⁻¹), the $f$ factor (0.9 rad R⁻¹), and the anisotropy factor (0.87). Normalized in this fashion, the dose rate for model 6711 at 6.0 cm was about 17% lower than that for model 6701.

*1983:* Another TLD study of the model 6701 dose distribution, this time in Mix D, was that of Hartmann *et al.*[61] They used lithium fluoride TLD's to measure the angular distribution of dose at various distances, both in Mix D and in air. Since they observed no systematic differences among the results at different distances, they averaged the Mix D data at each angle over distances from 0.5 cm to 5 cm and determined a best-fit quadratic function of angle, normalized at the transverse axis; they formulated a two-dimensional expression for dose by multiplying this angular distribution by the results of their transverse-axis TLD data in Mix D, which they multiplied by distance squared and least-squares fitted with a version of Berger's buildup equation, using the dose value at the origin as the scaling factor. From their article, it appears that the experimental data used in the fit were taken at distances from about 1.1 to 5.5 cm. Thus, the variation of dose with distance in the region less than 1 cm from the seed is determined entirely by the calculation, and the good agreement (differences of 1%–2%) they report with Krishnaswamy's results is not surprising. For the TLD's used (type not specifically identified), the response per unit dose in tissue relative to the $^{60}$Co response was determined (simulating $^{125}$I radiation by 40 kV x rays with 2 mm aluminum added filtration) to be 1.40 (±2.8%).

*1983:* Late in 1983, at about the same time as the introduction of the model 6711 $^{125}$I seed by the 3M Company, the National Bureau of Standards (NBS), now the National Institute for Standards and Technology (NIST), made available a standard for seed strength calibration in terms of exposure rate at 1 m on the transverse axis.[5] For all three seed types (models 6701, 6702, and 6711), the exposure rate at distances of 25 and 50 cm from an array of four to six closely spaced seeds was measured with a standard free-air chamber and the seeds were then introduced, one at a time, into a standard position in the center of a 20.3 cm diameter spherical aluminum re-entrant ion chamber. In this way, an ion chamber calibration factor was determined for each type of seed, by dividing the total measured ionization current from seeds in an array by the measured exposure rate at 1 m. Overall uncertainty in the calibration (95% confidence inter-

val) was estimated at 5%, 3%, and 4% for model 6701, 6702, and 6711 seeds, respectively. A user of the service would typically measure the response of a local re-entrant chamber to a selected seed before and after sending it to NBS (now NIST) for calibration in their spherical re-entrant chamber.

*1984*: For TLD's of lithium fluoride powder in throwaway capsules, Weaver[62] has used radiation from multiple model 6702 seeds to measure the response relative to that for $^{60}$Co at 1.39±0.03 (for dose to water) and 1.32±0.03 (for dose to muscle).

*1985*: Following the introduction of seed-strength standardization by NBS, Ling *et al.*[16] undertook a two-dimensional dosimetric study of the model 6711 seed similar, in some respects, to that by Hartmann *et al.*[61] for the model 6701. They measured the relative dose distribution as a function of angle between 0° and 90° from the seed axis and distances between 1 and 6 cm, both with a silicon diode detector in a water phantom and with 1 mm cube lithium fluoride TLD's in a Lucite phantom. When the TLD data were corrected for density and radiation absorption differences, using the Berger formalism, good agreement with the diode data was obtained. In contrast to the finding of Hartmann *et al.*[61] for the model 6701 seed, Ling *et al.*[6] found a variation in the radial distance dependence as a function of angle, with less angular dependence at greater distances. To accommodate this variation, they developed a "matrix fit" to their data, consisting of the product of a distance-dependent exponential with an angle-dependent extinction coefficient and a distance-dependent quadratic having angle-dependent coefficients, all divided by the square of the distance. A matrix of values tabulated for the four angle-dependent parameters includes data for angles of 0°, 60°, 70°, 80°, and 90° from the seed axis.

*1985*: Kubo[63] has called attention to the fact that 4.5 keV titanium K x rays emitted as fluorescent radiation from the capsule of $^{125}$I seeds can introduce error in strength (apparent activity) measurements using thin-window mammography ion chambers. Although these photons make no significant contribution to dose in water beyond about 1 mm from the seed, they are shown to contribute to exposure in air at 30 cm from the seed by about 4%. However, comparison performed at NBS resulted in differences of only 0.2% for a model 6711 seed and of 5% for a model 6702. Equatorial asymmetry (variation in exposure at different viewing angles in the transverse plane) was checked at 90° intervals and found to exhibit maximum differences of 8% for the model 6711 and 3% for the model 6702 seed.

*1986*: In a study that compared Monte Carlo calculated $^{125}$I with $^{60}$Co dose distributions in eye phantoms, Chiu-Tsao *et al.*[64] found a specific dose constant (Dale's definition[15]) in water of 1.33 cGy cm$^2$ mCi$^{-1}$ h$^{-1}$ at a point 1 cm toward the surface from a point source 2.5 cm inside a cylindrical head phantom. However, a subsequent recalculation using improved coherent scattering cross sections resulted in a lower value of 1.19 cGy cm$^2$ mCi$^{-1}$ h$^{-1}$ (private communication from Chiu-Tsao). Relative transverse-axis dose times the square of the distance along a phantom radius between source and surface displayed a peak at 0.8 cm from the

source at a value about 5% higher than the value at zero distance.

*1987*: A study very similar to the above work by Ling *et al.*[6] was reported by Schell *et al.*[7] for the model 6702 seed. Their measurements were made only in water with a silicon diode, extending to a 9 cm distance instead of 6 cm, as in the previous study, but the angles used and the method of data analysis were the same. In their discussion of the transverse axis data (normalized to 1.0 at 1 cm), they call attention to the agreement of their data with buildup factor calculations by the method of Berger and the fact that Monte Carlo data by Dale[15-17] are increasingly greater as a function of distance, i.e., about 60% greater at 9 cm.

*1987*: Burns and Raeside[65] in 1987, using their Monte Carlo code to study the model 6711 seed, obtained two-dimensional relative dose rate data very similar to that obtained by Williamson and Quintero.[27] As in their earlier study of the model 6702 seed, they calculated the dose rate in water per unit contained activity and suggested that the reader convert to dose rate per unit apparent activity by multiplying their data by the ratio of the dose rate at 1 cm from an encapsulated point source in water to the dose rate at 1 cm on the transverse axis of the seed; in this case, their value for that ratio was 2.0. Following their suggestion, and adjusting to earlier units for comparison, their value of the specific dose constant in water for this seed is 1.288 cGy cm$^2$ mCi$^{-1}$ h$^{-1}$, 11.6% higher than the value recommended by Williamson in 1988,[66] who had referenced his value to his own estimate of the NIST evaluation of air kerma strength, which explains 7% of the difference.

*1988*: A specific dose constant in water of 1.24 cGy cm$^2$ mCi$^{-1}$ h$^{-1}$ for a point source in a large, homogeneous water phantom resulted from Monte Carlo calculations by Williamson.[66] This work also included specific dose constants and relative dose factors along the transverse axis for realistic models of models 6701, 6702, and 6711 $^{125}$I seeds. The computer code permitted calculation, also, of the air kerma strength per unit contained activity for each seed type which, in turn, allowed the calculation of dose per unit air kerma strength rather than per unit contained activity. Specific dose constants determined were 1.21, 1.22, and 1.15 cGy cm$^2$ mCi$^{-1}$ h$^{-1}$, for the 6701, 6702, and 6711 seeds, respectively, where the dose rate per unit air kerma strength has been multiplied by 1.27 cGy cm$^2$ mCi$^{-1}$ h$^{-1}$ to permit comparison with values given previously in those units. These values include the influence of titanium $K$-shell x rays on the air kerma strength in Loftus' free-air chamber measurements of exposure rate,[5] which are simulated in these calculations; the effect is to reduce the calculated dose per unit air kerma strength by about 7%. Relative to the commonly assumed value[53] of 1.32 cGy cm$^2$ mCi$^{-1}$ h$^{-1}$ for muscle (1.28 cGy cm$^2$ mCi$^{-1}$ h$^{-1}$ for water), the above values are lower by 5.8%, 4.9%, and 11.3%, respectively, for the 6701, 6702, and 6711 seeds. In a subsequent report,[27] this study was expanded to produce complete two-dimensional dose distributions for seed models 6711 and 6702. Comparison with the experimental values of Ling *et al.*[6] for model 6711 and of Schell *et al.*[7] for model 6702 shows fairly good agreement (within 5%) except for very close to the source

and in the direction of the longitudinal axis, where differences of 10%–30% were observed. As for other Monte Carlo calculations (for example, by Dale,[15] Burns,[59] and Chiu-Tsao[64]), the relative dose increasingly exceeds measured results as the distance from the source is increased, a fact which the authors recognize but were unable to explain completely. Williamson[18] has shown that the explanation is a combination of replying on inaccurate photon cross-section libraries and the fact that Solid Water has significantly different radiological properties than liquid water.

*1988:* Herbolt et al.[67] reported results of Monte Carlo calculations of buildup factors in water in the photon energy range of 15 to 100 keV with special reference to ^{125}I seed dosimetry.

*1988:* Piermattei et al.[68] have reported their two-dimensional measurements in water, perspex, and three tissue substitute materials (muscle, adipose, and breast) for the model 6711 seed, using Harshaw lithium fluoride TLD chips ($3.1\times3.1\times0.89$ mm) and Kodak X-Omat V film. The TLD's were calibrated with x-ray beams of 27 and 34 keV effective energy and a response per unit exposure 1.27 times that for a ^{60}Co beam was observed at each energy. Transverse axis data were acquired with TLD's placed parallel to the seed axis with their centers in two spirals extending from 1 to 8 cm out from the seed in the central transverse plane of the seed. The film was used to get off-axis dose rate data. The authors found their relative dose rate data, both on and off the transverse axis, to not be significantly different from the data of Ling et al.[6] The specific dose constant found for both water and muscle substitute was $1.19$ cGy cm$^2$ mCi$^{-1}$ h$^{-1}$.

*1988:* Recently, Hashemi et al.[69] have determined an exposure rate constant for the model 6711 seed. The photon fluence rate on the transverse axis was evaluated using a collimated sodium iodide scintillation counter for a source of measured source strength, and photon energies and abundances were assigned using the data of Ling.[60] They determined an anisotropy factor in air of 0.88 and an effective exposure rate constant of $1.361$ R cm$^2$ mCi$^{-1}$ h$^{-1}$.

*1988:* An investigation by Meigooni et al.[26] of the suitability of three solid phantom materials for ^{125}I dose distribution measurements has shown that Solid Water results in a depth dose curve that is much closer to that calculated for pure liquid water medium than dose to water measured in PMMA or polystyrene phantoms. Polymethylmethacrylate (PMMA) results in a significantly slower dose falloff with distance and polystyrene produces a still slower falloff. They have shown that differences in dose falloff are not proportional to the density of the material and that the atomic composition of the phantom material is important. LiF TLD's (Harshaw lithium fluoride chips) were used for depth dose determinations in solid phantom materials, and the comparison was made on the basis of measurements in solid phantoms only and Monte Carlo calculations (using ITS code[70]) in solid phantoms as well as in water. Slower falloff is associated with greater photon energy degradation, as shown by Monte Carlo-generated energy histograms at 1, 5, and 10 cm depth. The conclusion is that Solid Water is a more suitable solid phantom material for dosimetry of ^{125}I than the other two materials.

*1989:* A combined TLD measurement and Monte Carlo calculation program has been carried out by Weaver et al.[8] with respect to model 6702 ^{125}I seeds, with measurements having been made, as well, for the model 6711 seed. In Solid Water phantom, a 5 mm$\times$2.2 mm capsule of lithium fluoride powder was placed at the center of a semicircular array of seeds having, in six successive measurements, radii ranging from 0.5 to 8.0 cm. The TLD material was calibrated against a thin-walled ion chamber of NIST-traceable calibration by irradiating each at the center of a 5 cm diameter ring of [125]I seeds. The Monte Carlo calculations (for water) of relative dose rate versus distance are about 15% higher than measured results by Meigooni et al.[26] One might expect near-perfect agreement if the calculation had assumed a Solid Water phantom. Relative measured data (normalized to 1.0 at 1 cm) for the model 6711 seed appear to show a value about 25% less at 8 cm than for the model 6702. Measured "dose factors" in Solid Water phantom (same as specific dose constant) were 1.18 and 1.06 cGy cm$^2$ mCi$^{-1}$ h$^{-1}$, respectively, for the 6702 and 6711 model seeds.

*1990:* Luxton et al.[71] elected to use a PMMA phantom for their transverse-axis TLD measurements to determine the specific dose constant in water of a model 6711 seed; they corrected the data to what would have been obtained in water by an adaptation of Berger's formalism. Measurements with 3 mm$\times$1 mm TLD-100 rods were performed at distances of 0.3, 0.5, and 1.0 cm from the seed. The specific dose constant was found to be $1.184$ cGy cm$^2$ mCi$^{-1}$ h$^{-1}$ in water, 4.6% less than that found in PMMA. A "scatter-attenuation" factor was defined to represent transverse axis dose rate with the effect of geometrical attenuation removed (a line source geometry factor was used with a 3 mm line length, which was not explicitly specified in their article). To the extent that the geometry factor was realistic, the variation with distance of this scatter-attenuation factor should be comparable to that of a water/air dose ratio for a point source. The value of the factor at 0.3 cm was 1.075 times the value at 1.0 cm.

*1990:* Transverse axis dose rates from 1.0 to 8.0 cm were measured by Nath et al.[9] in a Solid Water phantom, using lithium fluoride TLD chips, for both the model 6711 and the model 6702 seeds. Monte Carlo calculations using ITS code[70] were performed, as well, in Solid Water. The "dose rate constant," numerically equal to the specific dose constant but omitting the intrinsic distance squared factor, is defined as the dose rate per unit source strength at 1 cm distance on the transverse axis of the seed. Results obtained for the dose rate constants in a Solid Water phantom are $1.08\pm0.03$ and $1.14\pm0.03$ cGy mCi$^{-1}$ h$^{-1}$ for the 6711 and 6702 seeds, respectively, again using the older "apparent activity" mCi units for source strength to facilitate comparison with earlier results. In this work, the Monte Carlo calculations do agree with the measured dose rates throughout the range of distances considered.

*1990:* Measurements using both silicon diodes and lithium fluoride TLD's and calculations by the Monte Carlo method have been performed by Chiu-Tsao et al.[10] to determine dose rate distributions around ^{125}I sources. The diode

measurements were of water/air dose ratios as a function of distance on the transverse axis; they were made by lifting a water environment into place around the otherwise unperturbed detector and source in between two in-air readings. The ratios, inherently free of the geometry factor, clearly extrapolate to 1.0 at the seed center, where the dose rate (per unit source strength) divided by the geometry factor is expected to approach the product of the exposure rate constant and the $f$ factor, i.e., 1.28 cGy cm$^2$ mCi$^{-1}$ h$^{-1}$. At 1 cm, however, the ratios were 0.87 and 0.91, respectively, for the 6711 and 6702 seeds, indicating that the dose rate constants were approximately equal to the zero distance value multiplied by these factors. TLD's, in the form of 1 mm cubes for small distances and $3.1 \times 3.1 \times 0.89$ mm$^3$ chips for larger distances, were calibrated in air with radiation from an array of calibrated model 6702 seeds 7–20 cm distant. TLD data were acquired in two dimensions, at 10° intervals as a function of angle with respect to the source axis and at distances up to 10 cm. Transverse axis relative dose measurements in the range 2–8 cm had a maximum disparity of about 17% at 6 cm distance for the 6711 seed compared to the Monte Carlo calculations for water. There was good agreement (within ~5%) between calculations and measurements at distances less than 2 cm. A two-dimensional table based on calculated data for distances less than 2 cm were given for each of the two models of seed.

*1990*: In 1990, the ICWG (Chap. 3)[1] considered in detail the $^{125}$I dosimetry data generated by the three participating institutions, namely, Memorial Sloan-Kettering Cancer Center,[10] the University of California at San Francisco,[8] and Yale University.[9] It found Excellent agreement (within 3%) among the three and recommended an average of the three data sets for clinical use.[1] The ICWG recommended dose rate constants in Solid Water for $^{125}$I models 6702 and 6711 sources were 1.16 and 1.07 cGy mCi$^{-1}$ h$^{-1}$, respectively. The ICWG also noted that the value of 1.30 cGy mCi$^{-1}$ h$^{-1}$ in current use for both models of $^{125}$I sources is too high and needs to be revised. The ICWG noted that the radial dose function for the model 6711 source falls off slightly more rapidly than that for the model 6702 source, because of the presence of low-energy silver characteristic x rays in the spectrum of the model 6711 source. The anisotropy constants recommended for models 6702 and 6711 were 0.961 and 0.937, respectively. The radial dose function and anisotropy constants were also obtained by averaging the data from the three participating institutions.

*1990*: Cygler *et al.*[72] demonstrated using diode dosimetry and Monte Carlo simulations using the EGS4 code[73] that the presence of gold or silver backing near an $^{125}$I seed modifies the dose rate on the side away from the backing material. There is a small increase close to the gold, but a decrease of about 10% further away. Prior to this study several contradictory studies have been published.[74–78] More recently, Meli and Motakabbir[79] have investigated whether the $L$-shell characteristic x rays from the gold contribute to the increase in dose close to the gold backing material. Their results indicate that these soft x rays do not contribute significantly to the dose.

*1991*: Recently, Williamson[18] has reported a detailed com-

parison of the ICWG-measured dosimetry data for $^{125}$I in Solid Water with his Monte Carlo simulations in water as well as in Solid Water. This photon transport code allows realistic geometric simulation of the complex internal seed structure, NIST air kerma strength standardization geometry, and ICWG dose measurement setups. When the appropriate measurement medium and geometry were assumed, agreement between theory and measurement was excellent, within 3% at 1 cm and averaging 3% at larger distances. However, the data do not support the water equivalence of Solid Water at $^{125}$I energies, indicating that Solid Water measurements underestimate $^{125}$I specific dose rate constants in water by 4.3%. Because of its higher ratio of absorption to scatter, $^{125}$I dose distributions measured in Solid Water are less penetrating (by 35% at 10 cm) than those measured in liquid water. For model 6711 and model 6702 seeds, Monte Carlo calculations yielded specific dose rate constants (assuming liquid water medium) of 0.877 and 0.932 cGy cm$^2$ h$^{-1}$ per unit air kerma strength, respectively. For $^{125}$I, currently accepted values are 18% and 11% larger than values reported by Williamson[18] for the two seed models. We recommend the adoption of these values from Williamson[18] in this document.

*1993*: Recently, the anisotropy of dose distributions around $^{125}$I has been reexamined by Nath *et al.*[20] Dose rates around $^{125}$I model 6702 and 6711 sources were measured using LiF TLD's in a Solid Water phantom.[20] From these measured data, isodose rate contours were determined using a bivariate interpolation and smooth surface fitting algorithm. Also, $4\pi$-averaged anisotropy factors, $\phi_{an}(r)$, for use in a point-source approximation were calculated at radial distances varying from 1 to 10 cm for $^{103}$Pd, $^{125}$I, and $^{192}$Ir sources. The anisotropy factors increased slightly (less than 2%) with radial distance and had average values of 0.90, 0.94, 0.96, and 0.98 for $^{103}$Pd, $^{125}$I model 6711, $^{125}$I model 6702, and $^{192}$Ir, respectively. The anisotropy factors determined from dose measurements in phantom are observed to be closer to unity than from those determined previously from in-air measurements.[57,58,69] This can be attributed to the smoothing of two-dimensional dose distributions due to the presence of more scattered photons in the phantom measurements compared to in-air measurements. Because in-phantom measurements simulate more closely the brachytherapy patient, data from these experiments are recommended for a more accurate determination of dose distributions around clinical brachytherapy implants.

*1994*: Very recently, Luxton[80] reported calculations of dose rates around point sources of $^{125}$I and $^{103}$Pd in water and several water equivalent media using the EGS4 Monte Carlo code.[73] Correction factors to calculate dose in water medium were obtained for PMMA, Solid Water, and a material optimized for low-energy dosimetry (RW-1). For Solid Water, these correction factors are in good agreement with those reported earlier by Williamson.[18] For the $^{125}$I model 6711 source, the dose rate constant calculated by Luxton is 0.88 cGy h$^{-1}$ U$^{-1}$, which is in exact agreement with the value recommended by this task group.

## C. Palladium-103 sources

*1990*: Meigooni, Sabnis, and Nath[12] measured dose distributions around $^{103}$Pd sources using LiF TLD's in a Solid Water phantom. Measurements were performed for both model 100 and 200 sources. For the earlier $^{103}$Pd source design (model 100) about 30% of the dose at a distance of 5 cm was from high-energy and longer-lived radioisotopes created by activation of trace elements in the source materials and the encapsulation when the source assembly was irradiated in a nuclear reactor. To address this problem, the manufacturer developed the model 200 source, which is fabricated by irradiating $^{102}$Pd with thermal neutrons, followed by chemical purification and coating of the $^{103}$Pd on graphite cylinders, which are then hot loaded into titanium capsules. Meigooni *et al.*[12] showed that the new design source (model 200) does not suffer from the problems of trace elements. The dosimetry measurements were made in a two-dimensional Cartesian grid with a spacing of 0.5 cm for distances less than 3 cm and 1 cm for distances greater than 3 cm. The sensitivity of LiF TLD for $^{103}$Pd was assumed to be the same as that for $^{125}$I photons. The measured dose rate data were fitted to analytical expressions, and two-dimensional tables in both Cartesian and polar coordinates were generated. Dose rate constant in a Solid Water phantom for the $^{103}$Pd model 200 source was determined to be 0.735 ±0.03 cGy h$^{-1}$ U$^{-1}$, which is equivalent to 0.95±0.04 cGy h$^{-1}$ mCi$^{-1}$. The anisotropy constant in Solid Water was observed to have a value of 0.90. Radial dose function was also extracted from the measured data and fitted to an analytical expression.

*1991*: Dose measurements using LiF TLD's have also been performed by Chiu-Tsao and Anderson[19] for single $^{103}$Pd seeds (model 200) at the center of a Solid Water phantom. They used TLD cubes 1 mm on an edge for measurements from 1 mm to 1 cm at 1 mm intervals. The cubes were centered along transverse and longitudinal axes and along radial lines from seed center at 10° increments. TLD chips of 3.1×3.1×0.89 mm$^3$ dimension were used at distances of 2, 2.5, 3, and 4 cm at 15° angular intervals. They presented the product of distance squared and dose rate per unit source strength, plotted versus distance and angle. At 1 cm from seed center along the transverse axis this product was found to be 0.88 cGy cm$^2$ mCi$^{-1}$ h$^{-1}$, which is 8% smaller than the data presented by Meigooni *et al.*[12] One of the reasons for this discrepancy may be that Chiu-Tsao and Anderson[19] used homemade Solid Water, which may have had a slightly different composition than the commercial material used in Meigooni *et al.*'s work.[12] So far, the exact composition of the phantom material has not been specified.

*1991*: Results from the work of Chiu-Tsao and Anderson[19] were in good agreement (within 5%) with previous data of Meigooni *et al.*[12] for distances greater than 2 cm. The dose rate constant reported, however, was 7% smaller than that by Meigooni *et al.* Therefore, the task group chose to average these two data sets. Since both of these experiments used Solid Water, a correction for conversion of these data to liquid water was calculated using Monte Carlo simulation by Williamson.[18] He determined that the Solid Water needed to be multiplied by a factor of 1.048.

## APPENDIX D: GLOSSARY OF DEFINITIONS AND UNITS

| Symbol | Quantity | Units | Introduced |
|---|---|---|---|
| $A$ | Activity | Bq, mCi, Ci | App. A |
| $A_{app}$ | Apparent activity. | Bq, mCi | App. A |
| $B(\mu r)$ | Energy absorption buildup factor. | dimensionless | App. B |
| $d$ | Calibration distance from source, in transverse plane, where air kerma rate in free space is measured. | cm, m | II A |
| $d_0$ | Distance from source, in transverse plane, where reference exposure or air kerma rate is specified. | m | II A |
| $\dot{D}(r,\theta)$ | Dose rate at point $(r,\theta)$. | cGy h$^{-1}$ | II A |
| $f_{med}$ | Exposure-to-dose conversion factor. | cGy R$^{-1}$ | App. B |
| $F(r,\theta)$ | Anisotropy function at point $(r,\theta)$ | dimensionless | II A |
| $g(r)$ | Radial dose function. | dimensionless | II A |
| $g'(r)$ | Radial dose function for a point source. | dimensionless | App. B |
| $G(r,\theta)$ | Geometry factor at point $(r,\theta)$ | cm$^{-2}$ | II A |
| $I(r,\theta,L,t)$ | Sievert integral approximation to ratio of dose rate in water at $(r,\theta)$ from source of active length $L$ and filtration thickness $t$ to air kerma strength of a point source having some activity as given source. | cGy h$^{-1}$ U$^{-1}$, cm$^{-2}$ | App. B |
| $\dot{K}$ | Air kerma rate in free space. | cGy h$^{-1}$, $\mu$Gy h$^{-1}$ | II A |
| $\dot{K}_{wat}$ | Water kerma rate in free space. | cGy h$^{-1}$, $\mu$Gy h$^{-1}$ | App. B |
| $L$ | Active length of encapsulated source. | cm | II A |
| $M_{eq}$ | Equivalent mass of radium. | mg, mgRaEq | II A |
| $r$ | Distance from center of the active source. | cm | II A |
| $r_0$ | Reference distance from source center, generally 1 cm. | cm | II A |
| $R_x$ | Reference exposure rate. | R cm$^2$ h$^{-1}$ nR m$^2$ s$^{-1}$ mR m$^2$ h$^{-1}$ C kg$^{-1}$ m$^2$ s$^{-1}$ | App. A |
| $S(r,\theta)$ | Relative dose distribution, defined by Eq. (A1) | dimensionless | App. A |

| Symbol | Description | Units | Appendix |
|---|---|---|---|
| $S_k$ | Air kerma strength. | U<br>$\mu$Gy m$^2$ h$^{-1}$<br>cGy cm$^2$ h$^{-1}$ | III A |
| $t$ | Radial filter thickness. | mm | App. B |
| $T(r)$ | Ratio of dose in water to water kerma in free space for a point source at distance $r$. | dimensionless | App. B |
| $[W/e]$ | Mean energy expended per unit charge created in dry air. | cGy R$^{-1}$ J C$^{-1}$ | App. A |
| $\beta$ | Angle subtended by the active length at the point of interest, $P$. In Fig. 1, it is equal to $\theta_2 - \theta_1$. | degree, radian | II A |
| $(\Gamma_\delta)_k$ | Air kerma rate constant. $\delta$ refers to the low energy cutoff. | $\mu$Gy m$^2$ MBq$^{-1}$ h$^{-1}$ | App. A |
| $(\Gamma_\delta)_x$ | Exposure rate constant (except radium). $\delta$ refers to the low energy cutoff. | R cm$^2$ mCi$^{-1}$ h$^{-1}$ | App. A |
| $(\Gamma_\delta)_{x,Ra,t}$ | Exposure rate constant for $^{226}$Ra for thickness, $t$, of Pt encapsulation. $\delta$ refers to the low energy cutoff. | R cm$^2$ mg$^{-1}$ h$^{-1}$ | App. A |
| $\theta$ | Angle with respect to long axis of the source. | degree, radian | II A |
| $\theta_0$ | Reference axis of source, along which $g(r)$ is defined. Generally, $\theta_0 = \pi/2$, denoting the axis that bisects the long axis of the source. | degree, radian | II A |
| $\Lambda$ | Dose rate constant in a medium using air kerma strength normalization. | cGy h$^{-1}$ U$^{-1}$ | II A |
| $\Lambda_A$ | As above, except for apparent activity normalization. | cGy h$^{-1}$ mCi$^{-1}$ | App. A |
| $\Lambda_m$ | As above, except for equivalent mass of $^{226}$Ra normalization. | cGy h$^{-1}$ mgRaEq$^{-1}$ | App. A |
| $\mu$ | Linear attenuation coefficient of primary photons. | cm$^{-1}$ | App. B |
| $\mu'$ | Effective linear attenuation coefficient. | mm$^{-1}$ | App. B |
| $\mu_{en}/\rho$ | Mass energy absorption coefficient. | cm$^2$ g$^{-1}$ | App. B |
| $\rho(r)$ | Active source density, i.e., contained activity per unit volume. | Bq cm$^{-3}$ | II A |
| $\phi_{an}(r)$ | Anisotropy factor. | dimensionless | II A |
| $\bar{\phi}_{an}$ | Anisotropy constant. | dimensionless | II A |

## ACKNOWLEDGMENTS

The authors thank Anjali Nath and Deanna Jacobs for preparing this document and Anthony Melillo for the analysis of some of the data presented in this document. We would also like to thank Stuart Smolen for a careful reading of the manuscript and his suggestions.

[1] Interstitial Collaborative Working Group (ICWG), *Interstitial Brachytherapy: Physical, Biological, and Clinical Considerations*, edited by L. L. Anderson, R. Nath, and K. A. Weaver (Raven, New York, 1990).

[2] M. B. Podgorsak, L. A. DeWerd, and B. R. Paliwal, "The half life of high dose rate Ir-192 sources," Med. Phys. **20**, 1257–1259 (1993).

[3] G. P. Glasgow and L. T. Dillman, "Specific-ray constant and exposure rate constant for $^{192}$Ir," Med. Phys. **6**, 49–52 (1979).

[4] T. Altzitzoglou, "The half life of $^{125}$I," Appl. Radiat. Isot. **42**, 493–494 (1991).

[5] T. P. Loftus, "Exposure standardization of $^{125}$I seeds used for brachytherapy," J. Res. Natl. Bur. Stand. **89**, 295–303 (1984).

[6] C. C. Ling, M. C. Schell, E. D. Yorke, B. B. Palos, and D. O. Kubiatowicz, "Two-dimensional dose distribution of $^{125}$I seeds," Med. Phys. **12**, 652–655 (1985).

[7] M. C. Schell, C. C. Ling, Z. C. Gromadzki, and K. R. Working, "Dose distribution of model 6702 $^{125}$I seeds in water," Int. J. Radiat. Oncol. Biol. Phys. **13**, 795–799 (1987).

[8] K. A. Weaver, V. Smith, D. Huang, C. Barnett, M. C. Schell, and C. C. Ling, "Dose parameters of $^{125}$I and $^{192}$Ir seed sources," Med. Phys. **16**, 636–643 (1989).

[9] R. Nath, A. S. Meigooni, and J. A. Meli, "Dosimetry on the transverse axis of $^{125}$I and $^{192}$Ir interstitial brachytherapy sources," Med. Phys. **17**, 1032–1040 (1990).

[10] S.-T. Chiu-Tsao, L. L. Anderson, K. O'Brien, and R. Sanna, "Dose rate determination for $^{125}$I seeds," Med. Phys. **17**, 815–825 (1990).

[11] E. Browne and R. B. Firestone, *Table of Isotopes* (Wiley, New York, 1986).

[12] A. S. Meigooni, S. Sabnis, and R. Nath, "Dosimetry of $^{103}$Pd brachytherapy sources for permanent implant," Endocurietherapy Hypertherm. Oncol. **6**, 107–117 (1990).

[13] AAPM Report No. 21, *Recommendations of AAPM Task Group 32: Specification of Brachytherapy Source Strength* (American Institute of Physics, New York, 1987).

[14] J. F. Williamson and R. Nath, "Clinical implementation of AAPM Task Group 32 recommendations on brachytherapy source strength specification," Med. Phys. **18**, 439–448 (1991).

[15] R. G. Dale, "A Monte Carlo derivation of parameters for use in the tissue dosimetry of medium and low energy nuclides," Br. J. Radiol. **55**, 748–757 (1982).

[16] R. G. Dale, "Some theoretical derivations relating to the tissue dosimetry of brachytherapy nuclides, with particular reference to $^{125}$I," Med. Phys. **10**, 176–183 (1983).

[17] R. G. Dale, "Revisions to radial dose function data for $^{125}$I and $^{137}$Cs," letter to Med. Phys. **13**, 963–964 (1986).

[18] J. F. Williamson, "Comparison of measured and calculated dose rates in water near I-125 and Ir-192 seeds," Med. Phys. **18**, 776 (1991).

[19] S.-T. Chiu-Tsao and L. L. Anderson, "Thermoluminiscent dosimetry for $^{103}$Pd (Model 200) in solid water phantom," Med. Phys. **18**, 449–452 (1991).

[20] R. Nath, A. S. Meigooni, P. Muench, and A. Melillo, "Anisotropy functions for $^{103}$Pd, $^{125}$I, and $^{192}$Ir interstitial brachytherapy sources," Med. Phys. **20**, 1465–1473 (1993).

[21] M. Boutillon and A. M. Perroche-Roux, "Reevaluation of the W value for electrons in dry air," Phys. Med. Biol. **32**, 2134 (1987).

[22] F. H. Attix and V. H. Ritz, "A determination of the gamma-ray emission of radium," J. Res. Natl. Bur. Stand. **59**, 293–305 (1957).

[23] M. J. Berger, "Energy deposition in water by photons from point isotropic sources," MIRD pamphlet No. 2, J. Nucl. Med. Suppl. No. 1, 15–25 (1968).

[24] G. S. Burns and D. E. Raeside, "Monte Carlo simulation on the dose distribution around a commercial $^{125}$I seed," Med. Phys. **15**, 56–60 (1988).

[25] L. L. Meisberger, R. Keller and, R. J. Shalek, "The effective attenuation in water of the gamma rays of $^{198}$Au, $^{192}$Ir, $^{137}$Cs, $^{226}$Ra, and $^{60}$Co," Radiology **90**, 953–957 (1968).

[26] A. S. Meigooni, J. A. Meli, and R. Nath, "A comparison of solid phantoms with water for dosimetry of $^{125}$I brachytherapy sources," Med. Phys. **15**, 695–701 (1988).

[27] J. F. Williamson and F. J. Quintero, "Theoretical evaluation of dose distributions in water about models 6711 and 6702 $^{125}$I seeds," Med. Phys. **15**, 891–897 (1988).

[28] J. F. Williamson, "Monte Carlo and analytic calculation of absorbed dose near $^{137}$Cs intracavitary sources," Int. J. Radiat. Oncol. Biol. Phys. **15**, 227 (1988).

[29] B. L. Diffey and S. C. Klevenhagen, "An experimental and calculated

dose distribution in water around CDC *K*-type ^{137}Cs sources," Phys. Med. Biol. **20**, 446 (1975).

[30]F. J. Larke, "A practical improvement to the Sievert integral for more accurate dose distributions about iodine-125 brachytherapy seeds," M. S. thesis, the University of Colorado Health Sciences Center, Denver, CO, April, 1991.

[31]W. J. Meredith, D. Greene, and K. Kawashima, "The attenuation and scattering phantom of gamma rays from some radionuclides used in mould and interstitial gamma-ray therapy," Br. J. Radiol. **39**, 280–286 (1966).

[32]G. P. Glasgow, "Exposure rate constants for filtered ^{192}Ir sources," Med. Phys. **8**, 502–503 (1981).

[33]S. Webb and R. A. Fox, "The dose in water surrounding point isotropic gamma-ray emitters," Br. J. Radiol. **52**, 482–484 (1979).

[34]R. O. Kornelsen and M. E. J. Young, "Brachytherapy buildup factors," Br. J. Radiol. **54**, 136 (1981).

[35]A. L. Boyer, P. D. Cobb, K. R. Kase, and D. T. S. Chiu, "Ir-192 hospital calibration procedures," in *Recent Advances in Brachytherapy Physics*, edited by D. A. Shearer, AAPM Monograph 7 (American Institute of Physics, New York, 1981), pp. 82–103.

[36]T. P. Loftus, "Standardization of ^{192}Ir gamma ray sources in terms of exposure," J. Res. Natl. Bur. Stand. **85**, 19–25 (1980).

[37]W. P. M. Mayles and P. C. R. Turner, "The calculation of ^{192}Ir parameters for use in tissue dosimetry," letter to Br. J. Radiol. **56**, 606 (1983).

[38]A. D. Welsh, A. Dixon-Brown, and J. B. H. Stedford, "Calculation of dose distributions for ^{192}Ir implants," Acta Radiol. Oncol. **22**, 331–336 (1983).

[39]J. F. Williamson, R. L. Morin, and F. M. Khan, "Monte Carlo evaluation of Sievert integral for brachytherapy dosimetry," Phys. Med. Biol. **28**, 1021–1032 (1983).

[40]C. C. Ling, Z. C. Gromadzki, S. N. Rustgi, and J. H. Cundiff, "Directional dependence of radiation fluence from ^{192}Ir and [198]Au sources," Radiology **146**, 791–792 (1983).

[41]P. Kneschaurek and H. Lindner, "Dose and dose distribution close to ^{192}Ir sources," Strahlentherapie **161**, 706–710 (1985).

[42]J. A. Meli, A. S. Meigooni, and R. Nath, "On the choice of phantom material for the dosimetry of ^{192}Ir sources," Int. J. Radiat. Oncol. Biol. Phys. **14**, 587–594 (1988).

[43]A. S. Meigooni, J. A. Meli, and R. Nath, "Influence of the variation of energy spectra with depth in the dosimetry of ^{192}Ir using LiF TLD," Phys. Med. Biol. **33**, 1159–1170 (1988).

[44]M. T. Gillin, F. Lopez, R. W. Kline, D. F. Grimm, and A. Niroomand-Rad, "Comparison of measured and calculated dose distributions around a ^{192}Ir wire," Med. Phys. **15**, 915–918 (1988).

[45]G. Luxton, M. A. Astrahan, P. E. Liggett, D. L. Neblett, D. M. Cohen, and Z. Petrovich, "Dosimetric calculations and measurements of gold plaque ophthalmic irradiators using ^{192}Ir and ^{125}I seeds," Int. J. Radiat. Oncol. Biol. Phys. **15**, 167, 176 (1988).

[46]C. Thomason and P. Higgins, "Radial dose distribution of ^{192}Ir and ^{137}Cs seed sources," Med. Phys. **16**, 254–257 (1989).

[47]J. A. Meli, A. S. Meigooni, and R. Nath, "Comments on radial dose distribution of ^{192}Ir and ^{137}Cs seed sources," Med. Phys. **16**, 824 (1989) and reply to comments of Meil, Meigooni, and Nath, p. 825.

[48]C. Thomason, T. R. Mackie, M. J. Lindstrom, and P. D. Higgins, "The dose distribution surrounding ^{192}Ir and ^{137}Cs seed sources," Phys. Med. Biol. **36**, 475–493 (1991).

[49]C. Thomason, T. R. Mackie, and M. J. Lindstrom, "Effect of source encapsulation on the energy spectra of ^{192}Ir and ^{137}Cs seed sources," Phys. Med. Biol. **36**, 495–506 (1991).

[50]R. Loevinger, "Absorbed dose from interstitial and intracavitary sources," in DHEW Publication FDA-72-8024 Afterloading in Radiotherapy, Dept. of Health, Education, and Welfare (Rockville, MD, 1972), pp. 192–203.

[51]B. S. Hilaris, J. G. Holt, and J. St. Germain, *The Use of Iodine-125 for Interstitial Implants*, DHEW Publication (FDA) 76-8022 (U.S. Department of Health, Education and Welfare, Rockville, Maryland, 1975).

[52]L. L. Anderson, "Dosimetry for Interstitial Brachytherapy," in *Handbook of Interstitial Brachytherapy*, edited by B. S. Hilaris (Publishing Science Group, Acton, MA, 1975), pp. 87–115.

[53]J. G. Holt, D. J. Perry, and L. E. Reinstein, "The design of an ionization chamber to measure exposure in air for mammographic techniques," Med. Phys. **2**, 172 (1975), Abstract.

[54]L. L. Anderson and I. Y. Ding, "Dosimetry considerations for ^{125}I," in *Afterloading: 20 Years of Experience 1955–75*, edited by B. S. Hilaris

(Robert Gold and Assoc., New York, 1975), pp. 63–72.

[55]V. Krishnaswamy, "Dose distribution around an ^{125}I seed source in tissue," Radiology **126**, 489–491 (1978).

[56]C. C. Ling, L. L. Anderson, and W. U. Shipley, "Dose inhomogeneity in interstitial implants using ^{125}I seeds," Int. J. Radiat. Oncol. Biol. Phys. **5**, 419–425 (1979).

[57]C. C. Ling and P. J. Biggs, "Coincidence sum peak array of ^{125}I activity using solid state detectors," Med. Phys. **7**, 551–554 (1980).

[58]R. J. Schulz, P. Chandra, and R. Nath, "Determination of the exposure rate constant for ^{125}I using a scintillation detector," Med. Phys. **7**, 355–361 (1980).

[59]G. S. Burns and D. E. Raeside, "Monte Carlo simulation on the dose distribution around a commercial ^{125}I seed," Med. Phys. **15**, 56–60 (1988).

[60]C. C. Ling, E. D. Yorke, I. J. Spiro, D. Kubiatowicz, and D. Bennett, "Physical dosimetry of ^{125}I seeds of a new design for interstitial implant," Int. J. Radiat. Oncol. Biol. Phys. **9**, 1747–1752 (1983).

[61]G. H. Hartmann, W. Schlegel, and H. Scharfenberg, "The three-dimensional dose distribution of ^{125}I seeds in tissue," Phys. Med. Biol. **28**, 693–699 (1983).

[62]K. A. Weaver, "Response of LiF powder to ^{125}I photons," Med. Phys. **11**, 850–854 (1984).

[63]H. Kubo, "Exposure contribution from Ti *K* x rays produced in the titanium capsule of the clinical ^{125}I seed," Med. Phys. **12**, 215–220 (1985).

[64]S.-T. Chiu-Tsao, K. O'Brien, R. Sanna, H.-S. Tsao, C. Vialotti, Y. S. Chang, M. Rotman, and S. Packer, "Monte Carlo dosimetry for ^{125}I and ^{60}Co in eye plaque therapy," Med. Phys. **13**, 678–682 (1986).

[65]G. S. Burns and D. E. Raeside, "Two-dimensional dose distribution around ^{125}I seeds," Med. Phys. **14**, 420–424 (1987).

[66]J. F. Williamson, "Monte Carlo evaluation of specific dose constants in water for ^{125}I seeds," Med. Phys. **15**, 686–694 (1988).

[67]G. Herbold, G. Hartmann, H. Treuer, and W. J. Lorenz, "Monte Carlo calculation of energy buildup factors in the range from 15 to 100 keV, with special reference to the dosimetry of ^{125}I seeds," Phys. Med. Biol. **33**, 1037–1053 (1988).

[68]A. Piermattei, G. Arcovito, and F. Andreasi Bassi, "Experimental dosimetry of ^{125}I new seeds (mod. 6711) for brachytherapy treatments," Phys. Med. **1**, 59–70 (1988).

[69]A. M. Hashemi, M. D. Mills, K. R. Hogstrom, and P. R. Almond, "The exposure rate constant for a silver wire ^{125}I seed," Med. Phys. **15**, 228–234 (1988).

[70]J. Halbleib, "Structure and operation of the ITS code system," in *Monte Carlo Transport of Electrons and Photons*, edited by T. M. Jenkins, W. R. Nelson, and A. Rindi (Plenum, New York, 1988), pp. 249–262.

[71]G. Luxton, M. A. Astrahan, D. O. Findley, and Z. Petrovich, "Measurement of dose rate from exposure-calibrated ^{125}I seeds," Int. J. Radiat. Oncol. Biol. Phys. **8**, 1199–1207 (1990).

[72]J. Cygler, J. Szanto, M. Soubra, and D. W. O. Rogers, "Effects of gold and silver backings on the dose rate around an ^{125}I seed," Med. Phys. **17**, 172–178 (1990).

[73]W. R. Nelson and D. W. Rogers, "Structure and operation of the EGS-4 code system," in *Monte Carlo Transport of Electrons and Photons*, edited by T. M. Jenkins, W. R. Nelson, and A Rindi (Plenum, New York, 1988), pp. 287–306.

[74]G. Luxton, M. A. Astrahan, and Z. Petrovich, "Backscatter measurements from a single seed of ^{125}I for ophthalmic plaque dosimetry," Med. Phys. **15**, 397–400 (1988).

[75]K. A. Weaver, "The Dosimetry of ^{125}I seed eye plaques," Med. Phys. **13**, 73–83 (1986).

[76]A. Wu, E. S. Sternick, and D. J. Muse, "Effect of gold shielding on the dosimetry of an ^{125}I seed at close range," Med. Phys. **15**, 627–628 (1988).

[77]A. N. Harnett and E. S. Thomson, "An ^{125}I plaque for radiotherapy of the eye: Manufacture and dosimetric calculations," Br. J. Radiol. **61**, 835–838 (1988).

[78]S. T. Chiu-Tsao, L. L. Anderson, and I. Stabile, "TLD Dosimetry for ^{125}I eye plaque," Phys. Med. Biol. **33** Supp 1 (1988) 128 (abstract).

[79]J. A. Meli and K. A. Motakabbir, "The effect of lead, gold, and silver backings on dose near ^{125}I seeds," Med. Phys. A **20**, 1251–1256 (1993).

[80]G. Luxton, "Comparison of radiation dosimetry in water and in solid phantom materials for I-125 and Ir-192 brachytherapy sources: EGS4 Monte Carlo study," Med. Phys. **21**, 631–641 (1994).